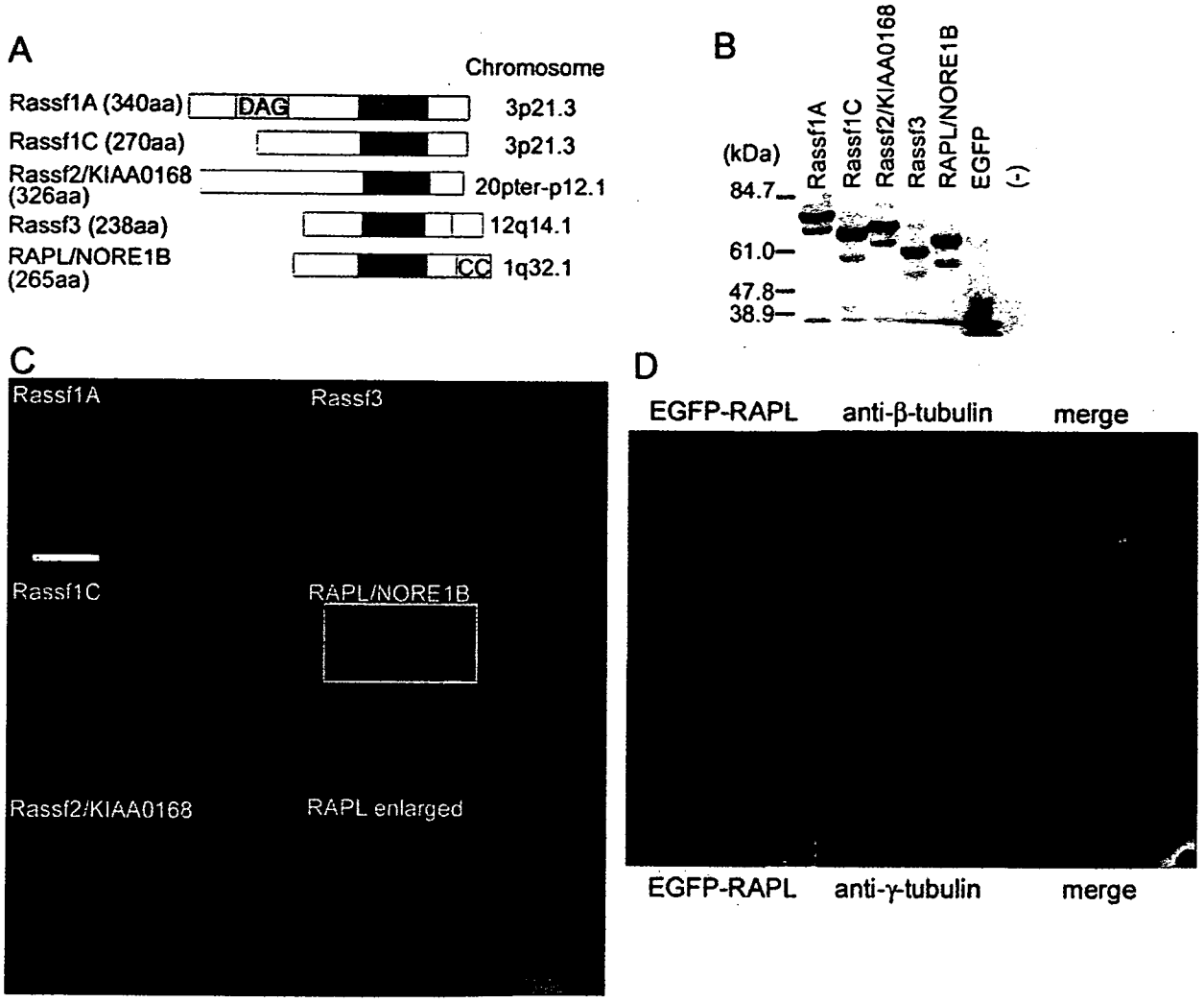

FIG. 2. **RAPL localizes to the microtubules in vascular endothelial cells.** *A*, Rassf members are schematically illustrated. All Rassfs contain a Ras/Rap1-associating domain (*RA*). Only Rassf1A contains the diacylglycerol-binding motif (*DAG*). Rassf3 and RAPL have coiled-coil domain (*CC*) in the carboxyl terminus. The localization of each gene to human chromosome is indicated on the *right*. *aa*, amino acids. *B*, HEK293T cells were transfected with EGFP-tagged plasmids as indicated at the *top*. Cell lysates were subjected to SDS-PAGE followed by immunoblotting with anti-GFP. −, untransfected. Molecular weight markers are indicated on the *left*. *C*, HAECs were transfected with the plasmids used in *B* and imaged through an Olympus IX81 fluorescent microscope. Note that EGFP-tagged Rassf1A and Rassf1C localize on the spiral fibers, whereas EGFP-tagged Rassf3 and RAPL localize at fibrous structures emanating from the center of the cell to the periphery. The tubular structure observed in HAECs expressing EGFP-RAPL is enlarged in the *right bottom panel*. Motile HAECs transfected with either EGFP-Rassf1A or EGFP-Rassf3 were video-imaged for phase contrast and EGFP. A series of phase-contrast images and EGFP images of each cell were converted to two videos, Supplemental Video 1 (phase contrast) and Supplemental Video 2 (EGFP). Elapsed time in video is indicated as h: min. Noticeably, the spiral structure surrounding the nucleus in the cell expressing Rassf1A does not move in the protrusive area at all. In clear contrast, the array from the center to the periphery of the cell expressing EGFP-Rassf3 moves toward the ruffled membrane, although both cells move spontaneously, similar to the untransfected cells. *Bar*, 20 μm. *D*, HAECs expressing EGFP-RAPL plated on a collagen-coated glass base dish were fixed with 4% paraformaldehyde, permeabilized with 0.1% Triton X-100, and incubated with anti-β-tubulin (*top*) or anti-γ-tubulin (*bottom*). Immunoreactive proteins were visualized by Alexa546 goat anti-mouse IgG. Both EGFP and Alexa546 images obtained through a BX50WI confocal microscope controlled by Fluoview are shown as RAPL (*green*), tubulin (*red*), and superimposed (*merge*). Note that EGFP-RAPL localizes on microtubules from the MTOC to the peripheral microtubules. *Bar*, 20 μm.

bules in HAECs expressing Rap1V12, whereas it localizes on microtubules in HAECs expressing rap1GAPII (Fig. 5*A*). These results suggested that activated Rap1 appears to determine the localization of RAPL. Thus, we investigated the effect of local activation of Rap1 on localization of EGFP-RAPL. Since vascular endothelial cells become motile upon S1P stimulation, S1P is thought to function as a chemoattractant (23). S1P did activate Rap1 as demonstrated by pull-down assay (Fig. 5*B*). GTP-Rap1 was increased at 1 min after S1P stimulation, and its activation persisted until 15 min after stimulation.

To examine the orientation of microtubule growth upon local S1P stimulation, we applied S1P to HAECs using micropipette. HAECs expressing EGFP-RAPL were monitored for cell movement and microtubule growth by phase-contrast and EGFP observations, respectively. HAECs cultured on the collagen-coated dish spontaneously moved around and exhibited prominent membrane ruffling, where the microtubules marked by EGFP-RAPL grew forward as shown by the *center panels* of Fig. 5*C*. The same cell was stimulated by 1 μM S1P released from the micropipette tip (Fig. 5*C*, *right panel*). The cell changed the direction of movement and showed remarkable membrane ruffles toward the pipette tip in response to S1P. Notably, microtubules marked by EGFP-RAPL started to grow in the protrusive area in the U-turned cell. The responses to S1P were constantly observed when HAECs were exposed to S1P from the tip of the micropipette. A series of phase-contrast images and EGFP images were converted to a video (Supplemental Video 3). We further confirmed the requirement of

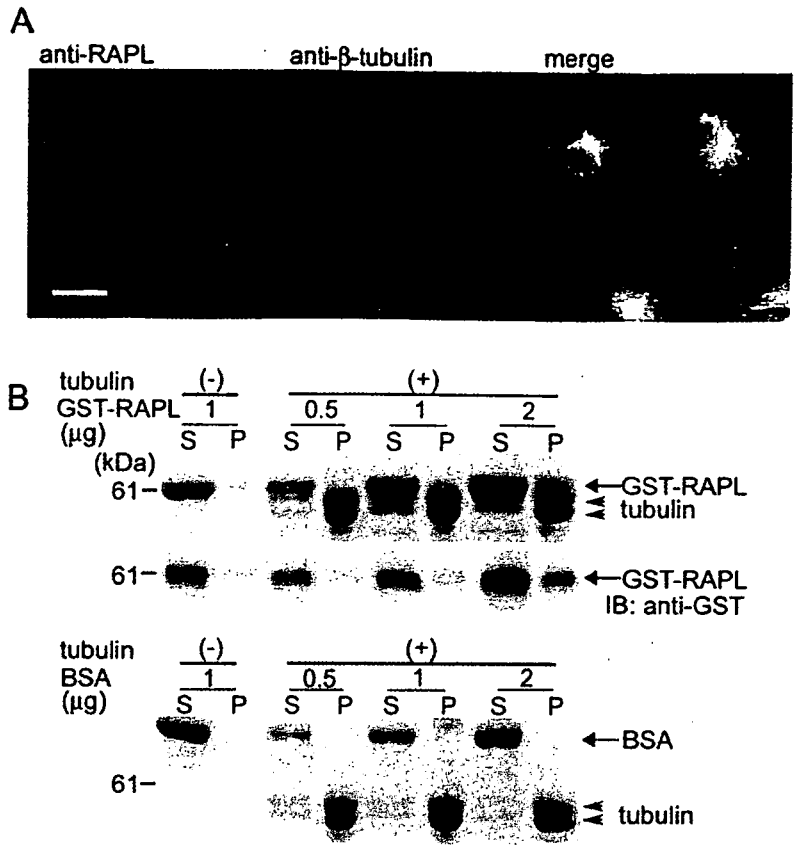

FIG. 3. **RAPL localizes on and binds to microtubules.** *A*, HAECs were immunostained with anti-RAPL antibody (*green*). Microtubules were visualized with immunostaining with anti-β-tubulin (*red*). A *merged image* is shown in the *right panel* (*merge*). *Bar*, 20 μm. *B*, GST-RAPL at the concentration as indicated at the *top* was mixed with 5 μg of purified tubulin (+) or without tubulin (−). After centrifugation at 400,000 × *g* for 30 min at 37 °C, supernatant (*S*) and pellet (*P*) were subjected to SDS-PAGE (*top panel*) followed by immunoblotting (*IB*) with anti-GST (*middle panel*). *Arrows*, *arrowheads*, and a *broken arrow* indicate GST-RAPL, tubulin, and bovine serum albumin (*BSA*), respectively. Note that GST-RAPL cosedimented with microtubules is detected in the pellet. To examine the specificity of the cosedimentation of GST-RAPL with microtubules, bovine serum albumin was used as a negative control in similar analyses to GST-RAPL (*bottom panel*).

microtubule growth for directional migration by examining whether endothelial cells extend membranes in response to S1P in the presence or absence of nocodazole. Before the nocodazole treatment, endothelial cells responded to S1P and extended their membranes, whereas after nocodazole, the cells did not extend their membranes (Supplemental Video 4). These data indicated that microtubules grow toward the chemoattractant, which promotes the directional cell movement.

To monitor the spatio-temporal activation of Rap1 in response to S1P from a micropipette, HAECs expressing Raichu-Rap1 were subjected to time lapse FRET imaging. Raichu-Rap1 consists of YFP, Rap1, the Ras-binding domain of Raf, CFP, and a CAAX box of Ki-Ras. This probe enabled us to show Rap1 activation by the increased ratio of YFP/CFP, based upon FRET from CFP to YFP (Fig. 5*D*). Raichu-Rap1-expressing HAECs exhibited remarkable membrane ruffles when stimulated with S1P from a micropipette (Fig. 5*E*, *third column*, *top*). At this time point, the increased FRET reflecting Rap1 activation was observed at the ruffled membrane (Fig. 5*E*, *third column*, *bottom*). When S1P was released from the relocated micropipette tip, the same cell responded to S1P and showed membrane ruffles toward the micropipette, similar to the first test. The similar Rap1 activation demonstrated by increased FRET was observed at the ruffled membrane (Fig. 5*E*, *right column*). A video image for both phase-contrast view and that for FRET images is shown as Supplemental Video 5. Rap1 activation at the ruffled membrane upon S1P stimulation was confirmed by the observation that Rap1 was not activated at the ruffled membrane before the S1P stimulation (Supplemental Fig. 2*A*). In addition, FRET observed at the ruffled membrane using Raichu-Rap1 was not detected when Raichu-Rap1N17 was used, although S1P-induced membrane ruffling was observed (Supplemental Fig. 2*B* and Video 6). By stimulating cells with S1P-free medium, we also excluded the possibility that fluid pressure or the proximity of the pipette tip to the cell might cause FRET (Supplemental Video 7). These data indicated that chemoattractant-induced local activation of Rap1 may become a trigger of directional migration accompanied by extension of EGFP-RAPL-marked microtubules.

Rap1 Activated during Wound Healing Is Accompanied by Microtubule Extension—To assess the consequence of the Rap1 activation and the association of activated Rap1 with RAPL, we examined the activation of RAPL and EGFP-RAPL-marked microtubules during wound healing. Microtubules grow in the protruding region of motile polarizing fibroblasts (28). It has been unclear what determines the polarized growth of microtubules. During wound healing, monolayer vascular endothelial cells migrated to the wound unidirectionally (Fig. 6*A*, *top panels*, phase-contrast observations). Crk is an adaptor protein linking signaling from integrins as well as receptor tyrosine kinases to its Src homology 3 domain-binding proteins via Src homology 2 domain. It localizes at focal adhesions by constituting complexes with Src homology 2 domain-binding partners, paxillin and p130Cas (29, 30). To monitor the focal adhesion assembly and growth of microtubules simultaneously, endothelial cells were transfected with the plasmids expressing DsRed-CrkI and EGFP-RAPL. Before scratching, DsRed-CrkI was punctually expressed in the focal adhesions at the cell periphery and the cell body (Fig. 6*A*, *bottom*, *left panel*). When cells started to move toward the wound, the focal complexes and focal adhesions marked by DsRed-CrkI developed profoundly in the leading edge of the cells (24, 31); meanwhile, those in the retracting region were disassembled (Fig. 6*A*, *bottom*, *right panel*). During cell migration upon scratching, microtubules marked by EGFP-RAPL grew in the protrusive region and developed toward the leading edge marked by DsRed-CrkI (Fig. 6*A*). A series of images for microtubules marked by EGFP-RAPL and those for focal adhesions marked by DsRed-CrkI were converted to a video file (Supplemental Video 8). We further confirmed that endogenous RAPL localized on microtubules in the protruding area of migrat-

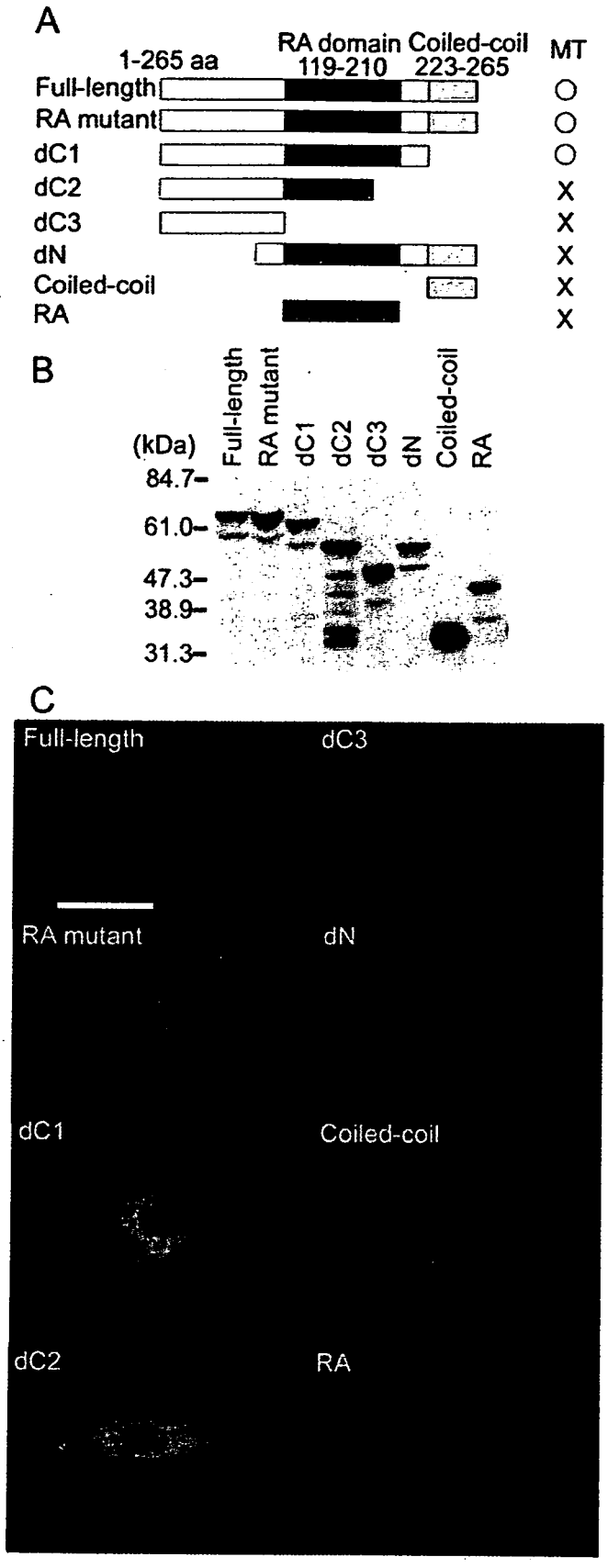

FIG. 4. **The sequence besides the essential amino acids in RA domain required for the association of RAPL with Rap1 is necessary for the localization of RAPL to microtubules.** *A*, schematic illustration of RAPL and its mutants. RAPL consists of an uncharacterized amino terminus, followed by a Ras/Rap1-associating domain (RA domain) and coiled-coil domain. The amino acid (*aa*) number encoding each domain is indicated at the *top*. *RA mutant*, the mutant incapable of associating with Ras and Rap1. The *stars* indicate the seven amino acids required for the association of RAPL with Rap1 that are replaced with Ala. dC1 and dC2 lacks the coiled-coil domain and both the RA domain and the coiled-coil domain, respectively. dC3 consists of the amino-terminal 100 amino acids. dN lacks the amino-terminal 100 amino acids, which have not been characterized. The coiled-coil and the RA consist of the only coiled-coil domain and the RA domain, respectively. The localization of RAPL and its mutants on microtubules is summarized on the *right*. *B*, HEK293T cells were transfected with the plasmids encoding amino-terminally EGFP-tagged DNA, as indicated at the *top*. Cell lysates were subjected to SDS-PAGE, followed by immunoblot probed with anti-GFP antibody. Molecular weight markers are indicated at the *left*. *C*, HAECs transfected with the plasmids used in *B* were imaged using an Olympus IX-81 fluorescent microscope. Note that RA mutant and dC1 localize on microtubules as well as full-length RAPL. *Bar*, 40 μm.

ing cells during wound healing (Fig. 6*B*).

Rap1 is activated downstream of Crk via its Src homology 3 domain-binding protein, C3G, which is a GEF for Rap1 (32). Thus, we examined whether Rap1 was activated during cell migration using Raichu-Rap1. HAECs cultured as a monolayer sheet were transfected with plasmids expressing Raichu-Rap1 and time lapse-imaged under the phase-contrast and FRET view after scratching. Cells were moving into the wound as revealed by phase-contrast observations (Fig. 7, *left panels*). Cell expressing Raichu-Rap1 as well as untransfected cells moved toward the wound. Rap1 was activated at the membrane ruffles in the leading edge (Fig. 7, *right panels*), where Crk was localized at focal complexes or growing focal adhesions (Fig. 6). These results suggested that Crk-Rap1 signaling upon focal adhesion assembly may contribute to the directional migration.

Rap1-RAPL Signaling Is Required for Directional Movement during Wound Healing—To test whether Rap1 is required for wound healing, we examined the effect of inactivation of Rap1 by overexpression of rap1GAPII on the directional cell migration. Rap family consists of Rap1A, Rap1B, Rap2A, and Rap2B (1). These molecules share common GEFs and GAPs for their activation and inactivation, respectively. To examine the effect of the Rap family on wound healing, inactivation of Rap by rap1GAPII, a common GAP for all of the Rap family members (33), is preferable rather than knocking down these Rap molecules using the small interfering RNA technique. In addition, rap1GAPII is suitable for the inactivation of Rap1, because it is reported that Rap1N17 does not work as a dominant negative form of Rap1 (34). HUVECs cultured as a monolayer were infected with adenovirus expressing either EGFP or rap1GAPII for 24 h. Infection efficiency exceeded 90%, as confirmed by fluorescence microscopy (Fig. 8*C*). There was no difference in cell confluence between HUVECs expressing rap1GAPII and those expressing EGFP. The EGFP-expressing cells separated by the wound moved toward the center line of the wound, whereas rap1GAPII-expressing HUVECs did not. The wound was almost closed by mobilized EGFP-expressing HUVECs 24 h after scratching, whereas it was not closed by rap1GAPII-expressing HUVECs (Fig. 8*A*).

To test the requirement of Rap1-RAPL signaling for directional movement, we used the RA mutant of RAPL to interfere with the association of RAPL with Rap1. HUVECs expressing EGFP-RA mutant were compared with those expressing EGFP-RAPL during wound healing. HUVECs infected with EGFP-RAPL-expressing adenovirus closed the wound 24 h after scratching, whereas those infected with EGFP-RA mutant-expressing adenovirus did not (Fig. 8*B*). To exclude the possibility that RA mutant-expressing cells moved more slowly than EGFP-expressing cells, we monitored randomly migrating cells expressing either RA mutant or EGFP. There was no significant change of the migratory velocity between two groups (Sup-

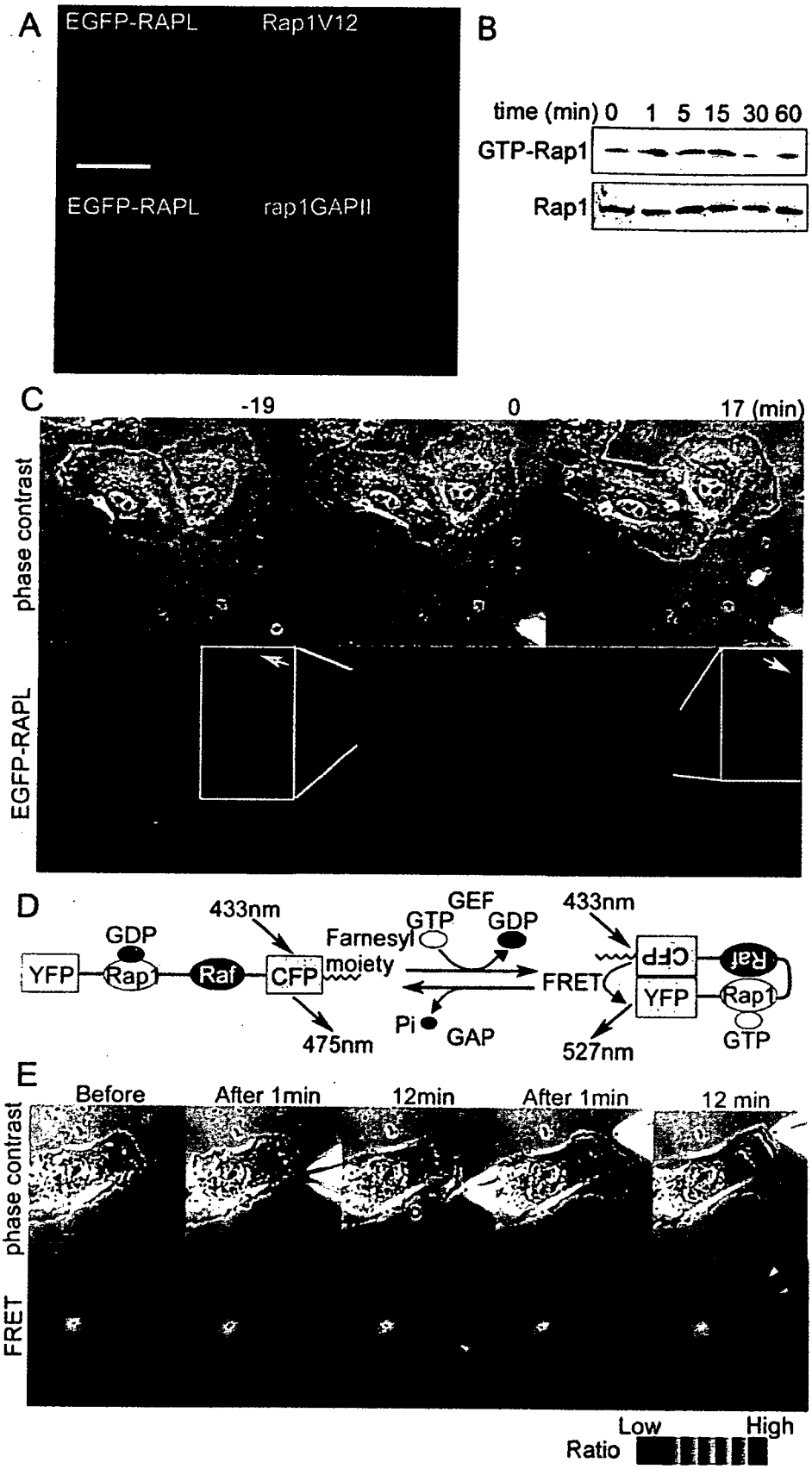

FIG. 5. **Rap1 regulates the localization of RAPL and precedes the extension of microtubules toward the leading edge of migrating cells upon chemotactic S1P stimulation.** *A*, HAECs were co-transfected with pCA-EGFP-RAPL and either pIRM21-Rap1V12 (*top*) or pIRM21-rap1GAPII (*bottom*). Note that EGFP-RAPL is dissociated from microtubules in Rap1V12-expressing cells, whereas EGFP-RAPL is associated with microtubules in rap1GAPII-expressing cells. *B*, HAECs stimulated with 1 μM S1P during the time period indicated at the *top* were lysed and analyzed by Bos's pull-down method using the GST-Rap1 binding domain of RalGDS. *C*, HAECs expressing EGFP-RAPL were time lapse-imaged before (−19 min) and after (17 min) the point (0) when 1 μM S1P was applied from a micropipette. Note that at time point 0, the cell

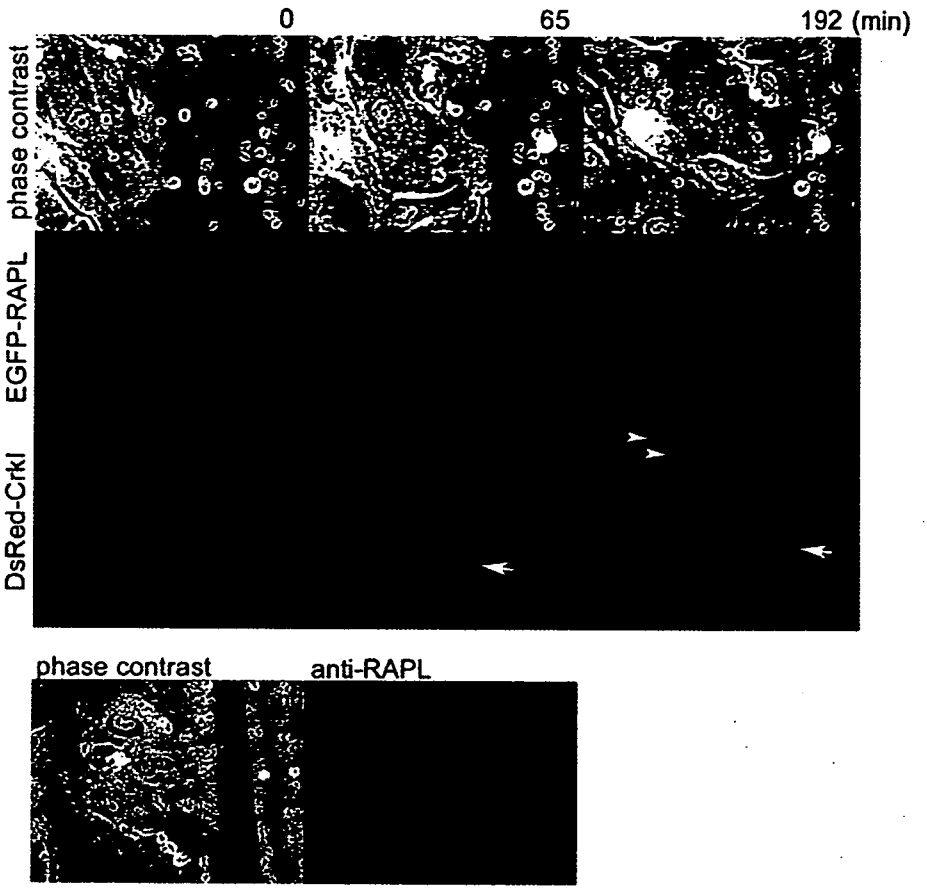

FIG. 6. **Microtubules marked by EGFP-RAPL grow toward the leading edge during wound healing.** *A*, monolayer-cultured HAECs expressing both EGFP-RAPL and DsRed-CrkI were time lapse-imaged after scratching. Phase-contrast (*top*), EGFP (*middle*), and DsRed (*bottom*) images were obtained through Olympus IX81 fluorescent microscope at the time point after scratching as indicated at the *top*. The *arrows* in the *bottom panel* indicate the nascent focal complexes at the leading edge, whereas the *arrowheads* indicate the focal adhesions in the retracting region. Note that microtubules marked by EGFP-RAPL grow toward the leading edge marked by DsRed-CrkI. *Wound*, scratched area. *Bar*, 50 μm. A series of time lapse images of phase-contrast, EGFP, and DsRed view were converted to a video (Supplemental Video 7). *B*, monolayer-cultured HAECs were immunostained with anti-RAPL 4 h after scratching. Phase contrast (*left*) and immunostaining with anti-RAPL (*right*) followed by visualization with Alexa488-conjugated secondary antibody are shown.

plemental Fig. 2*C*). These data indicated that Rap1 activation and subsequent Rap1-RAPL association is required for directional movement of endothelial cells during wound healing.

DISCUSSION

The directional migration is accompanied with microtubule growth toward the leading edge of migrating cells. The microtubule extension depends on the localization of microtubule-capturing or -attracting molecules. Microtubules cooperatively promote cell migration accompanied with cell polarization together with actin cytoskeleton (35, 36). Extracellular stimuli activating Rho family proteins, Rho, Rac, and Cdc42, via plasma membrane receptors and cell-ECM complexes determine the direction of microtubule growth (28). Therefore, the downstream effectors of Rho family proteins are proposed to function as microtubule-capturing molecules at the cell cortex. Such candidate systems include Cdc42-Par6-protein kinase Cζ-dynein and Rac/Cdc42-IQGAP-CLIP170 (35, 38). Here we demonstrate, for the first time, that Rap1-RAPL signaling contributes to determining the direction of cell migration accompanied with microtubule growth upon chemoattractant stimulation and during wound healing.

Given that RAPL was expressed in vascular endothelial cells and associated with GTP-Rap1, it is important to ask where and how RAPL is regulated by active Rap1 in living cells. To answer this question, we first examined the localization of RAPL and found that RAPL localized on microtubules from MTOC to the periphery. Previously, it has been reported that Rassf1A localizes on microtubules in a variety of cells (22) and participates in mitosis by inhibiting the binding of anaphase-promoting complex to Cdc20 (39) or by stabilizing microtubules for tumor suppression (22). Rassf members were originally isolated as tumor suppressors. Thus, Rassfs have been mainly focused on as regulators of tumor suppression. We noticed that microtubules found in HAECs transfected with pEGFP-Rassf1A and -1C were different from those found in HAECs transfected with pCA-EGFP-RAPL. Rassf1 appeared to deform and thicken microtubules, whereas RAPL seemed to localize on endogenous microtubules. Recently, Rassf1A and -1C are re-

moving toward the left top corner exhibited microtubules growing in the same direction as the cell movement. An *enlarged image* is shown in the *white box* (*bottom left*). Upon start of the S1P application, the cell turn to the micropipette tip (*black arrows*), began to move and exhibited a protrusion toward the tip, in which the microtubules extended forward along the direction of movement. An *enlarged image* is shown in the *white box* (*bottom right*). The *white arrows* indicate the moving direction. A series of phase-contrast images and EGFP images were converted into a video (Supplemental Video 3). *Bar*, 40 μm. *D*, schematic illustration of Raichu-Rap1. FRET efficiency depends on the guanine nucleotide binding. GDP-bound Raichu-Rap1 emits 475-nm fluorescence when excited at 433 nm, whereas GTP-bound Raichu-Rap1 emits 527-nm fluorescence due to FRET. *Raf*, Ras/Rap1 binding domain of Raf. *E*, HAECs expressing Raichu-Rap1 were imaged during exposure to S1P from the micropipette tip. Phase-contrast images and FRET images were obtained before and after the S1P stimulation. The time points indicated at the *top* show the first location and stimulation with S1P (*black*), the relocation of the tip, and the stimulation with S1P (*red*). Note that increased FRET reflecting Rap1 activation was observed at the edge of protrusion toward the micropipette tip. *Red* and *blue hue* indicate the increased and decreased FRET, respectively. The *arrowheads* indicate the activated Rap1 shown by the increased FRET. A series of phase-contrast images and FRET images were converted to a video (Supplemental Video 4). HAECs expressing Raichu-Rap1N17 was FRET-imaged during exposure to S1P from the micropipette tip similarly to Raichu-Rap1. Note that FRET does not occur at the ruffled membrane induced by S1P (Supplemental Video 5). Untransfected HAECs do not exhibit membrane ruffles in response to S1P-free medium (Supplemental Video 6).

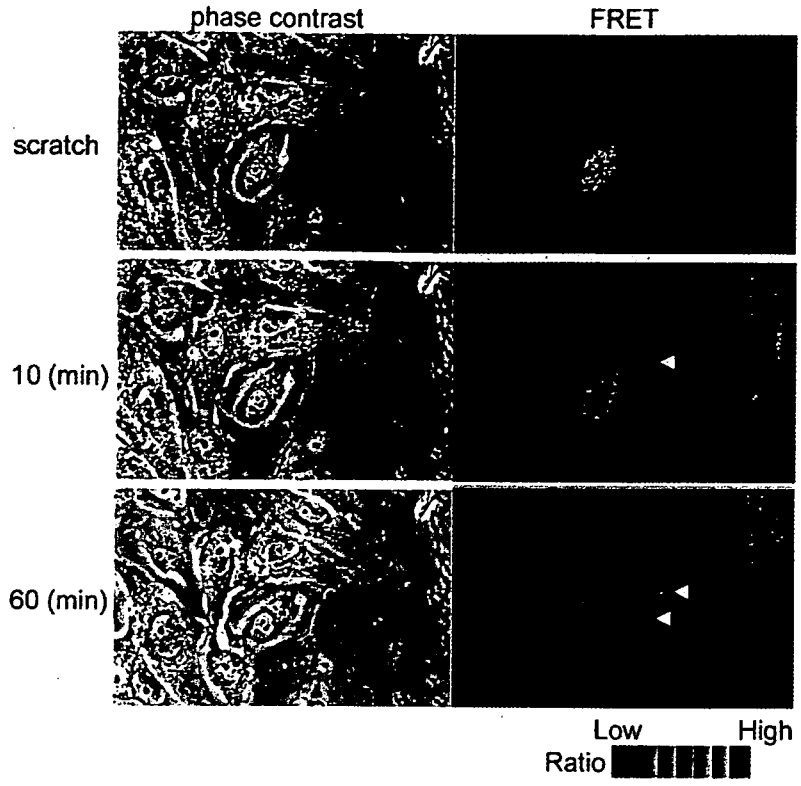

FIG. 7. **Rap1 is activated at the leading edge of the migrating cells.** HAECs cultured as a monolayer sheet transfected with pRaichu-Rap1 were scratched (*scratch*) and time lapse-imaged for phase-contrast and FRET observations. The elapsed time after scratching is indicated on the *left*. The *red hue* and *blue hue* in the FRET images indicate an increase (*high*) and a decrease (*low*) in the ratio of YFP to CFP, reflecting Rap1 activation and inactivation, respectively. The *arrowheads* indicate the activation of Rap1 at the leading edge of the cells migrating into the wound. The regions pointed out by the *arrows* are *enlarged* and shown in the *right corner* in the same *panel*. *Wound*, scratched area.

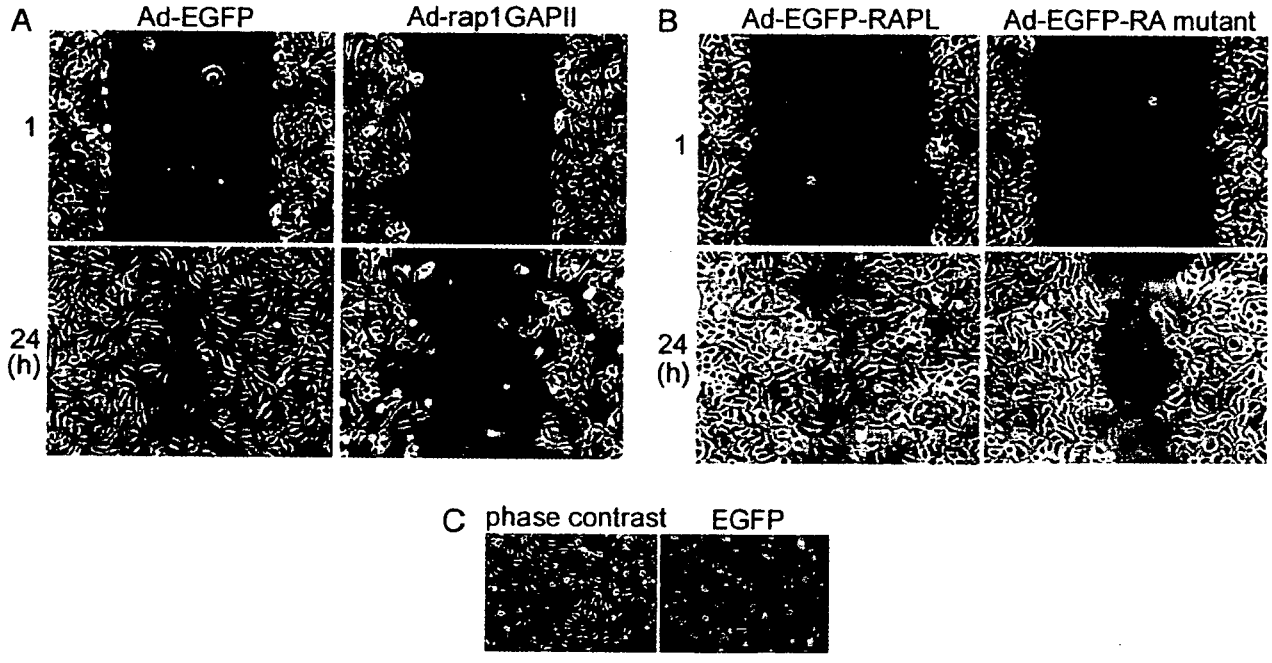

FIG. 8. **Rap1 activation and subsequent Rap1-RAPL association are required for wound healing.** *A*, HUVECs were either infected for 24 h with adenovirus expressing EGFP (Ad-EGFP) or adenovirus expressing rap1GAPII (Ad-rap1GAPII). 24 h after infection, the monolayer HUVECs were wounded by scratching. The wound healing was monitored at the time point as indicated on the *left*. Note that the cells expressing EGFP used as a control healed the wound, whereas the cells expressing rap1GAPII could not. HAECs infected with GFP-expressing adenovirus for 24 h were imaged. *B*, similarly to *A*, HUVECs were infected with either an adenovirus expressing EGFP-RAPL (Ad-EGFP-RAPL) or that expressing the EGFP-RA mutant of RAPL (Ad-EGFP-RA mutant). 24 h after scratching, cells were imaged. Note that the RAPL-expressing cells closed the wound, whereas those expressing RA mutant did not. *C*, the efficiency of infection was confirmed by the expression of EGFP in HUVECs infected with an adenovirus-expressing EGFP.

ported to suppress tumors by stabilizing microtubules and maintaining genomic stability (40). The circular fibers found in the EGFP-Rassf1-expressing cells appear to reflect the stabilized microtubules. Furthermore, although Rassf1A-transfected cells exhibited the membrane ruffling, microtubules marked by EGFP-Rassf1A did not grow or shrink at all (Fig. 2 and Supplemental Videos 1 and 2, *left*). In clear contrast, EGFP-tagged RAPL and endogenous RAPL localizes on microtubules (Figs. 2*D* and 3 and Supplemental Videos 1 and 3, *right*). RAPL dislocated from microtubules when cells were transfected with Rap1V12-expressing plasmids (Fig. 5*A*). In addition, inactivation of Rap1 and disconnection between Rap1 and RAPL perturbed the directional migration (Fig. 8). These results imply that Rap1-RAPL signal may participate in regu-

lation of microtubule growth. Further study is required to decipher the mechanism by which Rap1-RAPL-mediated signal regulates microtubule growth and/or stabilization.

Microtubules marked by EGFP-RAPL grew toward the leading edge, where DsRed-CrkI assembled as focal adhesions during wound healing. C3G is an Src homology 3 domain-binding protein of Crk and is required for stabilizing focal adhesions (7, 41). Thus, Rap1, a substrate of C3G, was likely to be activated at the assembly of focal adhesions. We used a FRET-based probe for visualizing Rap1 activation during wound healing. As expected, Rap1 was activated at the ruffled membrane where focal complexes were about to be assembled (Fig. 7). Thus, Rap1 activation at the leading edge preceded the directional migration. Rac1 activated downstream of CrkI via DOCK180 may tether microtubules through Rac1-binding protein, IQ-GAP1, and microtubule tip protein, CLIP-170 (42).

Microtubules have been suggested to target to focal adhesion, subsequently being captured and stabilized at focal adhesions (14, 15). We have not revealed the complex of Rap1-RAPL-microtubule at focal adhesions; however, Rap1 stabilizes focal adhesions, thereby indirectly contributing to the extension of microtubules. We have previously shown that Rap1 tightens the adhesion of cell-ECM complex (7) and that Rap1 is involved in maturation of focal complex to focal adhesions (24). RAPL was dislocated from the microtubules when constitutive active Rap1 was expressed (Fig. 5A). Katagiri *et al.* (16) reported that RAPL stabilizes the integrin-mediated cell attachment in lymphocytes stimulated with SDF-1. Accordingly, Rap1 activated at the focal adhesion may associate with RAPL, thereby stabilizing integrin-mediated focal adhesion to which microtubules target.

S1P triggers membrane ruffling, a hallmark of cell migration (26). We demonstrated that Rap1 was activated at S1P-induced membrane ruffling (Fig. 5). Membrane ruffling is the reorganization of actin by activated Rac. Rac activation downstream of Rap1 was previously reported in the Rap1-dependent secretory pathway (43). Rap1 promotes membrane extension by activating Rac via Vav2 and Tiam1 (44). Very recently, RIAM has been found to bind GTP-bound Rap1 and enhance integrin-mediated cell adhesion by regulating actin cytoskeleton (45). Thus, Rap1 appears to extend membranes by not only stabilizing integrin-mediated cell adhesion but activating Rac. Notably, microtubules marked by EGFP-RAPL grew toward locally activated Rap1 by S1P in the ruffled membrane. Although it is uncertain whether Rac activation is required for Rap1-RAPL-mediated signaling, Rac activation by S1P in parallel with or downstream of Rap1 may contribute to microtubule extension where RAPL localizes.

FRET-based probes, which can be introduced into living cells, have enabled us to monitor the spatial and temporal activation of signaling molecules: the activation of Ras superfamily members upon EGF-stimulation (4), the involvement of Crk in S1P-triggered signaling (26), and Rac activation during cell migration (37). We have previously shown that the phosphorylation of Crk was prominent at the S1P-induced membrane ruffling in vascular endothelial cells (26). Therefore, Rap1 activation by S1P in the present data is consistent with our previous data in that Crk-Rap1 signaling is triggered by S1P. During wound healing, Crk accumulated at focal adhesions and focal complexes near the leading edge. Although we could show Rap1 activation at the leading edge, it will be necessary to monitor the precise local activation of Rap1 at focal adhesions.

In conclusion, we have demonstrated that locally activated Rap1 regulates the directional cell migration accompanied by microtubule extension, presumably by dissociating RAPL from microtubules.

Acknowledgments—We thank M. Matsuda for advice; N. Yamagishi for the purified microtubules; H. Kurose and S. Hattori for the EGFP-expressing adenovirus and the rap1GAPII-expressing adenovirus, respectively; T. Kinashi for the anti-RAPL antibody; J. T. Pearson for critical reading of the manuscript; and M. Sone, M. Miyabayashi, K. Yamamoto, and N. Irisawa for technical assistance.

REFERENCES

1. Bos, J. L. (1998) *EMBO J.* **17**, 6776–6782
2. Bos, J. L., de Rooij, J., and Reedquist, K. A. (2001) *Nat. Rev. Mol. Cell. Biol.* **2**, 369–377
3. Ohba, Y., Kurokawa, K., and Matsuda, M. (2003) *EMBO J.* **22**, 859–869
4. Mochizuki, N., Yamashita, S., Kurokawa, K., Ohba, Y., Nagai, T., Miyawaki, A., and Matsuda, M. (2001) *Nature* **411**, 1065–1068
5. Reedquist, K. A., Ross, E., Koop, E. A., Wolthuis, R. M., Zwartkruis, F. J., van Kooyk, Y., Salmon, M., Buckley, C. D., and Bos, J. L. (2000) *J. Cell Biol.* **148**, 1151–1158
6. Katagiri, K., Hattori, M., Minato, N., Irie, S., Takatsu, K., and Kinashi, T. (2000) *Mol. Cell. Biol.* **20**, 1956–1969
7. Ohba, Y., Ikuta, K., Ogura, A., Matsuda, J., Mochizuki, N., Nagashima, K., Kurokawa, K., Mayer, B. J., Maki, K., Miyazaki, J., and Matsuda, M. (2001) *EMBO J.* **20**, 3333–3341
8. Kinbara, K., Goldfinger, L. E., Hansen, M., Chou, F. L., and Ginsberg, M. H. (2003) *Nat. Rev. Mol. Cell. Biol.* **4**, 767–776
9. Park, H. O., Sanson, A., and Herskowitz, I. (1999) *Genes Dev.* **13**, 1912–1917
10. Knox, A. L., and Brown, N. H. (2002) *Science* **295**, 1285–1288
11. Pollard, T. D., and Borisy, G. G. (2003) *Cell* **112**, 453–465
12. Ridley, A. J., Schwartz, M. A., Burridge, K., Firtel, R. A., Ginsberg, M. H., Borisy, G., Parsons, J. T., and Horwitz, A. R. (2003) *Science* **302**, 1704–1709
13. Small, J. V., Geiger, B., Kaverina, I., and Bershadsky, A. (2002) *Nat. Rev. Mol. Cell. Biol.* **3**, 957–964
14. Krylyshkina, O., Anderson, K. I., Kaverina, I., Upmann, I., Manstein, D. J., Small, J. V., and Toomre, D. K. (2003) *J. Cell Biol.* **161**, 853–859
15. Kaverina, I., Rottner, K., and Small, J. V. (1998) *J. Cell Biol.* **142**, 181–190
16. Katagiri, K., Maeda, A., Shimonaka, M., and Kinashi, T. (2003) *Nat. Immunol.* **4**, 741–748
17. Hesson, L., Dallol, A., Minna, J. D., Maher, E. R., and Latif, F. (2003) *Oncogene* **22**, 947–954
18. Vos, M. D., Martinez, A., Ellis, C. A., Vallecorsa, T., and Clark, G. J. (2003) *J. Biol. Chem.* **278**, 21938–21943
19. Vos, M. D., Ellis, C. A., Bell, A., Birrer, M. J., and Clark, G. J. (2000) *J. Biol. Chem.* **275**, 35669–35672
20. Vos, M. D., Ellis, C. A., Elam, C., Ulku, A. S., Taylor, B. J., and Clark, G. J. (2003) *J. Biol. Chem.* **278**, 28045–28051
21. Shivakumar, L., Minna, J., Sakamaki, T., Pestell, R., and White, M. A. (2002) *Mol. Cell. Biol.* **22**, 4309–4318
22. Liu, L., Tommasi, S., Lee, D. H., Dammann, R., and Pfeifer, G. P. (2003) *Oncogene* **22**, 8125–8136
23. Lee, M. J., Thangada, S., Paik, J. H., Sapkota, G. P., Ancellin, N., Chae, S. S., Wu, M., Morales-Ruiz, M., Sessa, W. C., Alessi, D. R., and Hla, T. (2001) *Mol. Cell* **8**, 693–704
24. Nagashima, K., Endo, A., Ogita, H., Kawana, A., Yamagishi, A., Kitabatake, A., Matsuda, M., and Mochizuki, N. (2002) *Mol. Biol. Cell* **13**, 4231–4242
25. Franke, B., Akkerman, J. W., and Bos, J. L. (1997) *EMBO J.* **16**, 252–259
26. Endo, A., Nagashima, K., Kurose, H., Mochizuki, S., Matsuda, M., and Mochizuki, N. (2002) *J. Biol. Chem.* **277**, 23747–23754
27. Kogata, N., Masuda, M., Kamioka, Y., Yamagishi, A., Endo, A., Okada, M., and Mochizuki, N. (2003) *Mol. Biol. Cell* **14**, 3553–3564
28. Wittmann, T., and Waterman-Storer, C. M. (2001) *J. Cell Sci.* **114**, 3795–3803
29. Schaller, M. D., and Parsons, J. T. (1995) *Mol. Cell. Biol.* **15**, 2635–2645
30. Vuori, K., Hirai, H., Aizawa, S., and Ruoslahti, E. (1996) *Mol. Cell. Biol.* **16**, 2606–2613
31. Webb, D. J., Parsons, J. T., and Horwitz, A. F. (2002) *Nat. Cell Biol.* **4**, E97–E100
32. Kiyokawa, E., Mochizuki, N., Kurata, T., and Matsuda, M. (1997) *Crit. Rev. Oncog.* **8**, 329–342
33. Mochizuki, N., Ohba, Y., Kiyokawa, E., Kurata, T., Murakami, T., Ozaki, T., Kitabatake, A., Nagashima, K., and Matsuda, M. (1999) *Nature* **400**, 891–894
34. van den Berghe, N., Cool, R. H., Horn, G., and Wittinghofer, A. (1997) *Oncogene* **15**, 845–850
35. Rodriguez, O. C., Schaefer, A. W., Mandato, C. A., Forscher, P., Bement, W. M., and Waterman-Storer, C. M. (2003) *Nat. Cell Biol.* **5**, 599–609
36. Goode, B. L., Drubin, D. G., and Barnes, G. (2000) *Curr. Opin. Cell Biol.* **12**, 63–71
37. Itoh, R. E., Kurokawa, K., Ohba, Y., Yoshizaki, H., Mochizuki, N., and Matsuda, M. (2002) *Mol. Cell. Biol.* **22**, 6582–6591
38. Gundersen, G. G. (2002) *Nat. Rev. Mol. Cell. Biol.* **3**, 296–304
39. Song, M. S., Song, S. J., Ayad, N. G., Chang, J. S., Lee, J. H., Hong, H. K., Lee, H., Choi, N., Kim, J., Kim, H., Kim, J. W., Choi, E. J., Kirschner, M. W., and Lim, D. S. (2004) *Nat. Cell Biol.* **6**, 129–137
40. Vos, M. D., Martinez, A., Elam, C., Dallol, A., Taylor, B. J., Latif, F., and Clark, G. J. (2004) *Cancer Res.* **64**, 4244–4250
41. Caron, E., Self, A. J., and Hall, A. (2000) *Curr. Biol.* **10**, 974–978
42. Fukata, M., Watanabe, T., Noritake, J., Nakagawa, M., Yamaga, M., Kuroda, S., Matsuura, Y., Iwamatsu, A., Perez, F., and Kaibuchi, K. (2002) *Cell* **109**, 873–885
43. Maillet, M., Robert, S. J., Cacquevel, M., Gastineau, M., Vivien, D., Bertoglio, J., Zugaza, J. L., Fischmeister, R., and Lezoualc'h, F. (2003) *Nat. Cell Biol.* **5**, 633–639
44. Arthur, W. T., Quilliam, L. A., and Cooper, J. A. (2004) *J. Cell Biol.* **167**, 111–122
45. Lafuente, E. M., van Puijenbroek, A. A., Krause, M., Carman, C. V., Freeman, G. J., Berezovskaya, A., Constantine, E., Springer, T. A., Gertler, F. B., and Boussiotis, V. A. (2004) *Dev. Cell* **7**, 585–595

Long-Term and Sustained COMP-Ang1 Induces Long-Lasting Vascular Enlargement and Enhanced Blood Flow

Chung-Hyun Cho, Kyung Eun Kim, Jonghoe Byun, Hyung-Suk Jang, Duk-Kyung Kim, Peter Baluk, Fabienne Baffert, Gyun Min Lee, Naoki Mochizuki, Jin Kim, Byeong Hwa Jeon, Donald M. McDonald, Gou Young Koh

Abstract—Vascular enlargement is a characteristic feature of angiopoietin-1 (Ang1)-induced changes in adult blood vessels. However, it is unknown whether tissues having Ang1-mediated vascular enlargement have more blood flow or whether the enlargement is reversible. We have recently created a soluble, stable and potent Ang1 variant, COMP-Ang1. In the present study, we investigated the effects of varied dose and duration of COMP-Ang1 on vascular enlargement and blood flow in the tracheal microvasculature of adult mice and explored a possible mechanism of long-lasting vascular enlargement. We found that COMP-Ang1 administered by adenoviral vector induced long-lasting vascular enlargement and increased tracheal blood flow. In contrast, short-term administration of COMP-Ang1 recombinant protein induced transient vascular enlargement that spontaneously reversed within a month. In both cases, the vascular enlargement resulted from endothelial proliferation. The COMP-Ang1–induced vascular remodeling is mediated mainly through Tie2 activation. Sustained overexpression of Tie2 could participate in the maintenance of vascular changes. Together, our findings indicate that sustained treatment with COMP-Ang1 can produce long-lasting vascular enlargement and increased blood flow. (***Circ Res.*** **2005;97:86-94.)**

Key Words: angiopoietin-1 ■ COMP-Ang1 ■ vascular enlargement ■ blood flow

Angiopoietin-1 (Ang1) is known to be a ligand to Tie2 tyrosine kinase receptor expressed on endothelial cells.[1] Ang1/Tie2 signaling is thought be involved in branching and remodeling of the primitive vascular network and in the recruitment of mural cells during development.[2,3] Transgenic overexpression of Ang1 using the skin-specific keratin-14 promoter produces leakage-resistant and enlarged vessels with an increased number of endothelial cells in skin.[4,5] Gene transfer of Ang1 into ischemic tissues produces notably enlarged blood vessels.[6,7] Baffert et al recently identified that Ang1-induced vascular enlargement could be the result of endothelial proliferation in trachea mucosa.[8] Thus, a cardinal feature of Ang1-induced vascular remodeling is vascular enlargement resulting from endothelial cell proliferation in adult animals.[4–8]

Given that Ang1-induced therapeutic benefits correlated with vascular enlargement in the ischemic tissues,[6,7,9] enhanced blood flow through blood vessels enlarged by Ang1 treatment could provide a great therapeutic benefit to ischemic peripheral tissues. However, it is not known whether the tissues having Ang1-mediated enlarged vessels have more blood flow. In addition, the effective dose and treatment period of Ang1 for inducing effective vascular enlargement is not known. Moreover, it is not known whether Ang1-mediated vascular enlargement regresses when Ang1 stimulation is withdrawn.

We have recently developed a soluble, stable, and potent Ang1 variant, COMP-Ang1.[10] To create this protein, we replaced the amino-terminal portion of Ang1 with the short coiled-coil domain of cartilage oligomeric matrix protein (COMP). COMP-Ang1 is more potent than native Ang1 in phosphorylating the Tie2 receptor and signaling via Akt in primary cultured endothelial cells.[10]

In the present study, we investigated effects of period and dose of COMP-Ang1 on vascular enlargement and tissue blood flow in adult mice and investigated a possible mechanism for long-lasting vascular enlargement induced by long-term and sustained COMP-Ang1. To determine the underly-

Original received March 29, 2005; resubmission received May 10, 2005; revised resubmission received June 8, 2005; accepted June 8, 2005.

From the Biomedical Research Center and Department of Biological Sciences (C.-H.C., K.E.K., G.M.L., G.Y.K), Korea Advanced Institute of Science and Technology, Daejeon, Korea; the Department of Medicine (J.B., H.-S.J., D.-K.K.), Samsung Medical Center and Samsung Biomedical Research Institute, Sungkyunkwan University School of Medicine, Seoul, Korea; the Cardiovascular Research Institute, Comprehensive Cancer Center, and Department of Anatomy (P.B., F.B., D.M.M.), University of California, San Francisco; the Department of Structural Analysis (N.M.), National Cardiovascular Center Research Institute, Suita, Osaka, Japan; the Department of Anatomy (J.K.), College of Medicine, The Catholic University of Korea Seoul; and the Department of Physiology (B.H.J), College of Medicine, Chungnam National University Daejeon, Korea.

Correspondence to Gou Young Koh, Biomedical Research Center, Korea Advanced Institute of Science and Technology, 373-1, Guseong-dong, Daejeon, 305-701, Republic of Korea. E-mail gykoh@kaist.ac.kr

© 2005 American Heart Association, Inc.

Circulation Research is available at http://circres.ahajournals.org

DOI: 10.1161/01.RES.0000174093.64855.a6

ing mechanism of COMP-Ang1–stimulated vascular remodeling in adult mice, we focused on the microvasculature of the trachea, which is distinguished by its simplicity and monolayer structure. Our results indicate that long-term and sustained COMP-Ang1 produced by adenoviral delivery of COMP-Ang1 induces a long-lasting vascular enlargement and enhanced blood flow without enhanced pericyte recruitment in adult mice. Long-lasting Tie2 expression could be involved in the long-lasting vascular enlargement and enhanced blood flow.

Materials and Methods

Generation of COMP-Ang1 Recombinant Protein and Ade-COMP-Ang1

Recombinant Chinese hamster ovary cells expressing COMP-Ang1 (CA1–2; production rate, ≈30 mg/L) were established as previously described.[11] Recombinant adenovirus expressing COMP-Ang1 or LacZ was constructed using the pAdEasy vector system (Qbiogene). For additional Materials and Methods, see online data supplement at http://circres.ahajournals.org.

Animals, Treatment, and Measurement of Blood Pressure and Heart Rate

Specific pathogen-free FVB/N mice and Tie2-GFP transgenic mice (FVB/N)[12] were purchased from Jackson Laboratory and bred in our pathogen-free animal facility. Male mice 8 to 10 weeks old were used for this study. Animal care and experimental procedures were performed under approval from the Animal Care Committees of the Korea Advanced Institute of Science and Technology. For protein treatment, 200 μg of COMP-Ang1 recombinant protein or BSA dissolved in 50 μL of sterile 0.9% NaCl was injected daily through the tail vein for 2 weeks. For adenoviral treatment, the indicated amount of Ade-COMP-Ang1, Ade-LacZ, or Ade-sTie2-Fc (generous gift from Drs Gavin Thurston and Ella Ioffe at Regeneron Pharmaceuticals, Terrytown, NY) diluted in 50 μL of sterile 0.9% NaCl was injected intravenously through the tail vein. Systemic blood pressure and heart rate were measured under anesthesia.

Enzyme-Linked Immunosorbent Assay

Approximately 50 μL of blood was obtained from the tail vein into a heparinized capillary tube at the indicated times. ELISA was adopted for precise detection of COMP-Ang1 in plasma.

Immunohistochemical Staining

Mice were anesthetized, perfused with 1% paraformaldehyde in PBS, and several organs including tracheas were removed. Tracheas and ear skins were immunostained as whole mounts, whereas other organs were immunostained as sections. Signals were visualized, and digital images were obtained with a Zeiss Apotome microscope and a Zeiss LSM 510 confocal microscope.

Measurement of Tracheal Tissue Blood Flow

After the mice were anesthetized, a type N flowprobe (Transonic Systems Inc, Ithaca, NY) was placed on tracheal wall along second, third, and forth cartilage rings without applying pressure, as this would occlude the vessels and reduce perfusion in the area of interest. The flowprobe was kept in place on the position of the highest sensitivity by a micromanipulator and connected to a laser-Doppler flowmeter (model BLF21; Transonic Systems Inc), which can measure microcirculation in 1 mm^3 of tissue for real-time assessment of perfusion (mL/min per 100 g of tissue).

Morphometric Measurements and Statistics

Morphometric measurements of the vessel diameters and area densities in mouse trachea were made as previously described.[13] For each trachea, the numbers of PH3-immunopositive endothelial cells, platelet/endothelial cell adhesion molecule (PECAM)-1–immunopositive blood vessels, and desmin/NG2-immunopositive pericytes were measured in 5 regions, each 0.21 mm^2 in area. Values were expressed per millimeter squared. Values presented are mean±SD. Significance of differences between mean was tested by analysis of variance followed by the Student–Newman–Keuls test. Statistical significance was set at $P<0.05$.

Results

Systemic Adenoviral COMP-Ang1 Produces Differential Enlargements of Blood Vessels in Mouse Tracheal Mucosa

For in vivo treatments with COMP-Ang1, we developed a stable Chinese hamster ovary cell line (CA1–2) which produces COMP-Ang1 at ≈30 mg/L. The potency, solubility, oligomerization status, and stability of the COMP-Ang1 produced from CA1–2 are similar to those of COMP-Ang1 produced from COS-7 cells transiently transfected with plasmid vector containing the COMP-Ang1 gene[10] (data not shown). Adult mice were treated with a daily intravenous injection of 200 μg of COMP-Ang1 recombinant protein or BSA through the tail vein for 2 weeks, then blood vessels in the tracheal mucosa were visualized with PECAM-1 immunostaining (Figure 1). Six segments of the microvasculature were distinguished by their position in the vascular hierarchy and differences in endothelial cell morphology.[14] Enlargement of tracheal blood vessels was found in mice that received COMP-Ang1 in the following descending order of effect: postcapillary venules>capillaries>collecting venules>venules>terminal arterioles (Figure 1B). No significant change was noted in segmental arterioles. These phenomena were observed in all individuals of several mouse strains studied (FVB/N, C57BL/6, BALB/c, BALB/c-*nu*, C3H/HeJ). No changes in the sizes or shape of tracheal blood vessels were found in mice that received BSA.

Short-Term and Intermittent Circulating COMP-Ang1 Induces Reversible Enlargement of Postcapillary Venules and Arterioles in Tracheal Vessels

When 200 μg of COMP-Ang1 recombinant protein was injected intravenously into adult male mice, circulating COMP-Ang1 level peaked immediately after injection (≈3.75 minutes), then declined, and returned almost to the control level 3 to 4 hours after treatment (Figure 2A, left). The half-life ($t_{1/2}$) of circulating COMP-Ang1 was 11.8 minutes. Daily intravenous injection of 200 μg of COMP-Ang1 for 1 week in mice produced an ≈2.0-fold enlargement of postcapillary venules and a 1.4-fold enlargement of terminal arterioles in the trachea (Figure 2). The COMP-Ang1–induced enlargement of postcapillary venules, collecting venules, venous end of capillaries, venules, and terminal arterioles were further increased up to 2 weeks on continuation of daily injection of COMP-Ang1 for up to 2 weeks. However, COMP-Ang1–induced enlarged blood vessels returned gradually to normal after discontinuation of the COMP-Ang1 treatment (Figure 2). One month after discontinuation of the COMP-Ang1 treatment, a second round of treatment with a daily intravenous injection of 200 μg of COMP-Ang1 for 2 weeks induced similar enlargements

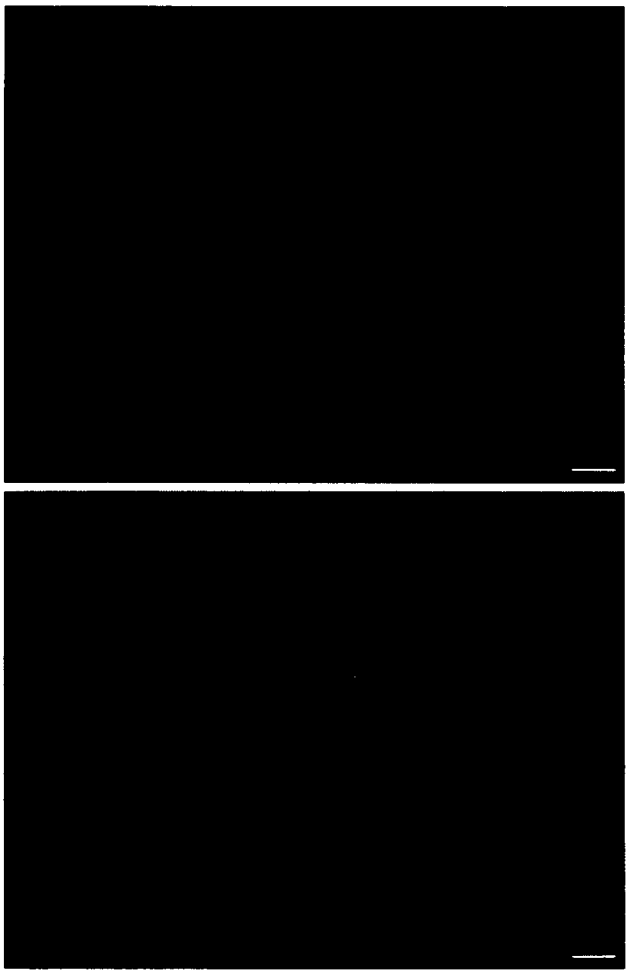

Figure 1. Effect of systemic COMP-Ang1 protein treatment on blood vessels in mouse tracheal mucosa. FVB/N mice were treated with daily injections of 200 μg of BSA (A) or 200 μg of COMP-Ang1 recombinant protein (B) for 14 days. Blood vessels in tracheal whole mounts were visualized with PECAM-1 (CD31) immunostaining (red). Six segments of the microvascular hierarchy are evident: segmental arteriole (sa, arrows), terminal arteriole (ta), capillary (cap), postcapillary venule (pcv), collecting venule (cv), and venule (ve). Of these, postcapillary venules and the venous ends of capillaries were the most enlarged after treatment by COMP-Ang1. The results from 4 experiments were similar. Scale bar=50 μm.

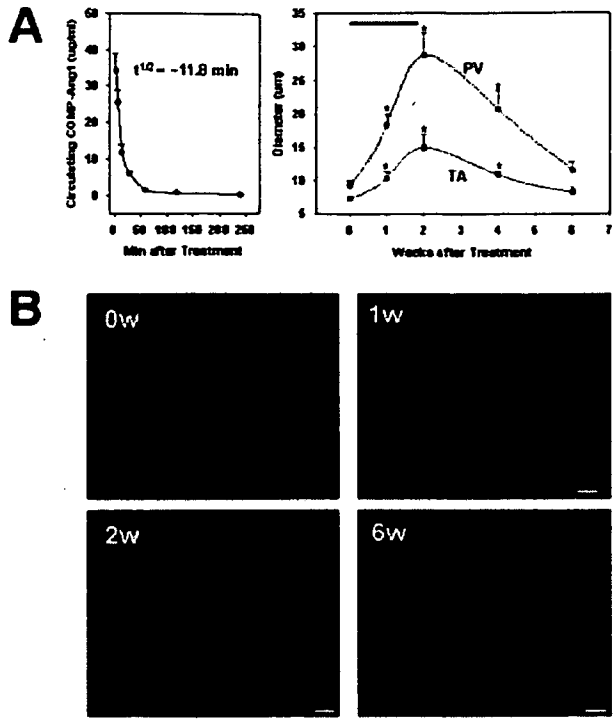

Figure 2. Effect of systemic COMP-Ang1 protein treatment on postcapillary venules and terminal arterioles. FVB/N mice were treated by daily injection of COMP-Ang1 recombinant protein (200 μg) for 14 days (A, black bar). At the indicated times, tracheal vessels were visualized with PECAM-1 immunostaining (B, red). The diameter of postcapillary venules and terminal arterioles are shown (A, right). Circulating plasma levels of COMP-Ang1 were measured by ELISA after a single injection of COMP-Ang1 recombinant protein (200 μg/mouse) (A, left). Diameters of 35 to 40 postcapillary venules (PV)/5 fields (brown curve) and 10 to 12 terminal arterioles (TA)/10 fields (blue curve) were measured at the edge of cartilage rings in each mouse. Values are mean±SD from 4 to 5 mice. *$P<0.05$ vs control period. COMP-Ang1 induced enlargement of postcapillary venules, collecting venules, venous ends of capillaries, venules, and terminal arterioles for up to 2 weeks, and then the enlarged blood vessels returned gradually to normal after discontinuation of the COMP-Ang1 treatment. Scale bar=50 μm.

of tracheal vessels, again in a reversible manner (data not shown). In comparison, the diameters of tracheal vessels were indistinguishable between the control and experimental periods in tracheal vessels of mice treated with BSA (data not shown). These results indicate that short-term spikes of circulating COMP-Ang1 induce reversible enlargement of some tracheal vessels.

Long-Term and Sustained Circulating COMP-Ang1 Induces Long-Lasting Enlargement of Postcapillary Venules and Terminal Arterioles in Tracheal Vessels

As an alternative method for systemic treatment with COMP-Ang1, an adenoviral vector encoding the COMP-Ang1 gene (Ade-COMP-Ang1) was developed. As a control, an adenoviral vector encoding the LacZ gene (Ade-LacZ) was developed. The potency, solubility, oligomerization status, and stability of the COMP-Ang1 produced from HEK293 cells transduced with Ade-COMP-Ang1 are similar to that of COMP-Ang1 produced from COS-7 cells transiently transfected with plasmid vector containing the COMP-Ang1 gene[10] (data not shown). Adult mice were treated with 1×10^9 pfu Ade-COMP-Ang1 or Ade-LacZ. At multiple times more than a period of 16 weeks, circulating plasma COMP-Ang1 levels were measured, and blood vessels in tracheal mucosa were visualized with PECAM-1 immunostaining (Figure 3). Circulating COMP-Ang1 increased as early as 12 hours after treatment, peaked at 1 to 2 weeks, declined gradually thereafter, and returned to control levels at 6 weeks after treatment (Figure 3A). The peak concentrations of circulating COMP-Ang1 were ≈3.5 to 4.5 μg. Significant enlargement of postcapillary venules, capillaries (distinctively, only the venous end of capillaries was enlarged), collecting venules, and terminal arterioles, but not segmental arterioles, was notice-

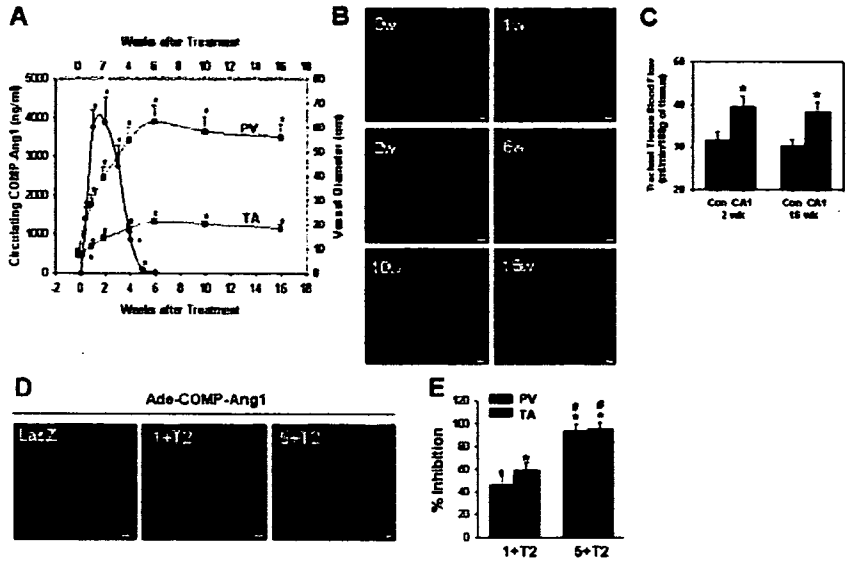

Figure 3. Effect of adenoviral COMP-Ang1 on postcapillary venules and terminal arterioles and blood flow. A through D, FVB/N mice were treated with 1×10^9 pfu Ade-COMP-Ang1 (n=6). At the indicated times, circulating plasma levels of COMP-Ang1 were measured by ELISA (A, black circle), and tracheal vessels were visualized with PECAM-1 immunostaining (B, red). The diameters of postcapillary venules (PV, brown curve) and terminal arterioles (TA, blue curve) are shown. Diameters of 35 to 40 PV/5 fields and 10 to 12 TA/10 fields were measured at the edge of cartilage rings in each mouse. Values are mean±SD from 4 to 5 mice. *$P<0.05$ vs control period. Scale bar=50 μm. C, Laser-Doppler flowmetric analyses for tracheal tissue blood flows of the mice treated with 1×10^9 pfu Ade-LacZ (Con) or 1×10^9 pfu Ade-COMP-Ang1 (CA1). Quantification of tracheal blood flows at 2 and 16 weeks after treatment with Con or CA1. Bars represent mean±SD from 4 to 5 mice. *$P<0.05$ vs Con. D and E, FVB/N mice were pretreated with 1×10^8 (1+T2) or 5×10^8 (5+T2) pfu Ade-sTie2-Fc (n=5 each), or 5×10^8 pfu Ade-LacZ (LacZ, n=5) at 24 hours before 1×10^8 pfu Ade-COMP-Ang1 treatment. Two weeks later, tracheal vessels were visualized by PECAM-1 immunostaining (D, red). Scale bar=50 μm. Diameters of 35 to 40 PV/5 fields and 10 to 12 TA/10 fields were measured at the edge of cartilage rings in each mouse. E, Bars represent the mean±SD from 5 experiments as percentage of inhibition of vascular remodeling induced by the pretreatment. Vascular remodeling induced by pretreatment of the Ade-LacZ is arbitrarily given as 100%. *$P<0.05$ vs LacZ, #$P<0.05$ vs 1+T2.

able at 1 week after the Ade-COMP-Ang1 treatment (Figure 3B). The vascular enlargements induced by Ade-COMP-Ang1 increased further for up to 6 weeks and then reached a plateau (Figure 3A and 3B). For example, the diameter of postcapillary venules increased 4.3-fold at 2 weeks, 6.0-fold at 4 weeks, and 6.8-fold at 6 weeks (Figure 3A). The enlargement of terminal arterioles was also significant beginning at 1 week after the treatment and increased in a time-dependent manner. However, the increase in diameter in terminal arterioles was less than that in postcapillary venules (Figure 3A and 3B). Importantly, the size of Ade-COMP-Ang1–induced enlarged blood vessels did not significantly decrease for as long as 16 weeks after the treatment, although circulating COMP-Ang1 returned to the control level at 6 weeks after treatment (Figure 3A). In comparison, diameters of tracheal vessels in mice treated with Ade-LacZ were indistinguishable between the control and experimental periods (data not shown). Using a laser-Doppler flowmeter, tracheal tissue blood flows were measured at 2 weeks (the peak level of circulating COMP-Ang1) and 16 weeks (undetectable level of circulating COMP-Ang1) after Ade-LacZ or Ade-COMP-Ang1 treatment. At 2 weeks, tracheal tissue blood flow was increased ≈25% in the mice treated with Ade-COMP-Ang1 compared with the mice treated with Ade-LacZ (Figure 3C and 3D). At 16 weeks, importantly, increased tracheal tissue blood flow by Ade-COMP-Ang1 was not significantly changed (Figure 3C and 3D). These results indicate that long term and sustained circulating COMP-Ang1 treatment induces long-lasting enlargement of tracheal blood vessels with long-lasting enhancement of tissue blood flow in the adult mice.

Tie2 Activation Is Involved in COMP-Ang1–Induced Vascular Remodeling

To determine the involvement of Tie2 activation in COMP-Ang1–induced vascular remodeling, the mice were pretreated with 1×10^8 pfu or 5×10^8 pfu Ade-sTie2-Fc at 24 hours before 1×10^8 pfu Ade-COMP-Ang1 treatment. Two weeks later, the diameters of postcapillary venules and terminal arterioles were measured. Pretreatment with 1×10^8 pfu or 5×10^8 pfu Ade-sTie2-Fc suppressed COMP-Ang1–induced vascular remodeling to the following extent: 46.5±7.7% or 93.5±6.4% in postcapillary venules and 59.7±6.6% or 95.1±5.7% in terminal arterioles, respectively (Figure 3E and 3F). These data indicate that COMP-Ang1–induced vascular remodeling is mainly mediated through Tie2 activation in adult tracheal vessels.

Long-Term and Sustained Circulating COMP-Ang1 Induces Various Vascular Remodeling in Different Organ

Both mice treated with Ade-LacZ (1×10^9 pfu) and those treated with Ade-COMP-Ang1 (1×10^9 pfu) appeared generally healthy, as they gained weight normally. However, the skin of mice treated with Ade-COMP-Ang1 appeared strikingly redder than the skin of mice treated with Ade-LacZ, beginning 10 to 14 days after the treatment. The Ade-COMP-

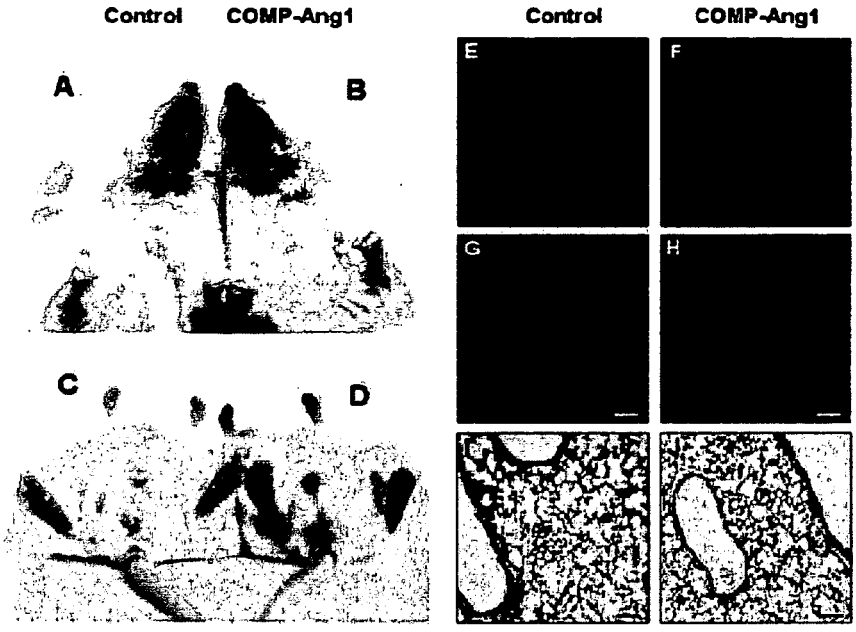

Figure 4. Effect of adenoviral COMP-Ang1 on skin color and vascular remodeling in ear skin and lung at 16 weeks after treatment. FVB/n mice were treated with 1×10^9 pfu Ade-LacZ or Ade-COMP-Ang1. Sixteen weeks later, the skin color of the face, hands, soles, penis, and tail were photographed (A, B, C, and B), blood vessels in ear skin (E and F) and lungs (G and H) were visualized with PECAM-1 (CD31) immunostaining (red), and sections of lungs were stained with H&E (I and J). The mice treated with Ade-COMP-Ang1 show overt skin redness, have prominently enlarged blood vessels in the ear skin, and have more dense PECAM-1–positive endothelial cells in the lung without overt histologic alteration compared with the mice treated with Ade-LacZ. The results from 4 experiments were similar. Scale bar=50 μm.

Ang1–induced skin redness persisted for as long as 16 weeks after the treatment (Figure 4). Sixteen weeks after the treatment, skin color in hair-sparse portions such as the face, hands, soles, penis, and tail of mice treated with Ade-COMP-Ang1 were distinctly redder than those of mice treated with Ade-LacZ. Blood vessels of the ear and capillaries of the heart, adrenal cortex, and liver of the mice treated with Ade-COMP-Ang1 were enlarged (Figures 4 and 5). More PECAM-1–positive endothelial cells were present in the lung, heart, liver, and renal medulla of mice treated with Ade-COMP-Ang1 compared with the mice treated with Ade-LacZ (Figures 4 and 5 and online Figure I in the data supplement). However, blood vessels of the renal cortex, including glomeruli, and intestinal villi of the mice treated with Ade-COMP-Ang1 and the mice treated with Ade-LacZ were indistinguishable. In addition, the body weights, systemic blood pressures, and heart rates of the 2 groups of mice were indistinguishable. These results indicate that long-term and sustained circulating COMP-Ang1 treatment induces long-lasting tissue-specific vascular remodeling in different blood vessels without notable changes in systemic blood pressure and heart rate (online Table I).

Induction of Tie2 Could Be Involved in Permanent Changes of COMP-Ang1–Induced Vascular Remodeling

Based on these observations, we asked whether Tie2 expression was more abundant in postcapillary venules than termi-

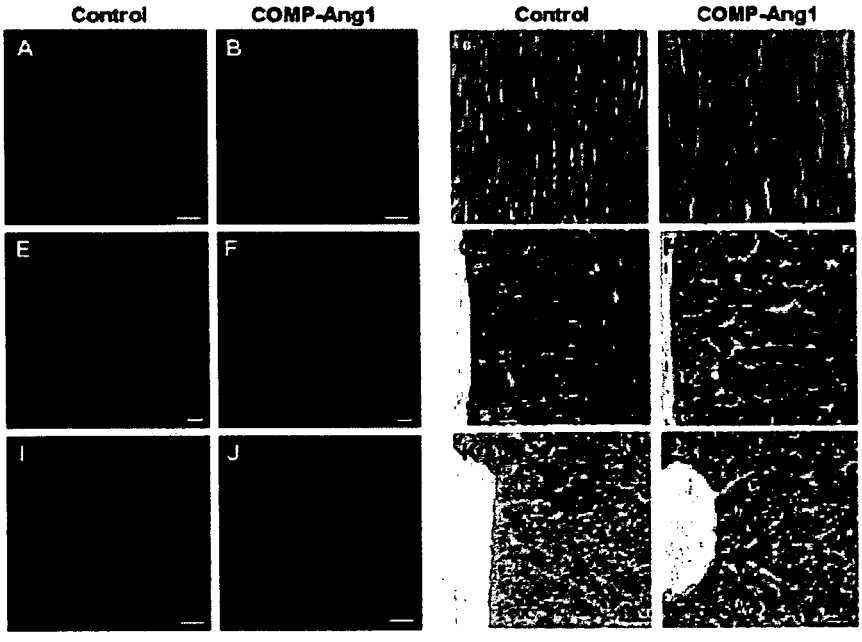

Figure 5. Effect of adenoviral COMP-Ang1 on vascular remodeling in heart, adrenal cortex, and liver at 16 weeks after the treatment. FVB/n mice were treated with 1×10^9 pfu Ade-LacZ or Ade-COMP-Ang1. Sixteen weeks later, blood vessels in heart (A through D), adrenal cortex (E through H), and liver (I through L) were visualized with PECAM-1 (CD31) immunostaining (red), and the sections were stained with H&E. The mice treated with Ade-COMP-Ang1 have enlarged capillaries in the heart and adrenal cortex and more PECAM-1–positive endothelial cells in the liver compared with the mice treated with Ade-LacZ. The results from 4 experiments were similar. Scale bar=25 μm.

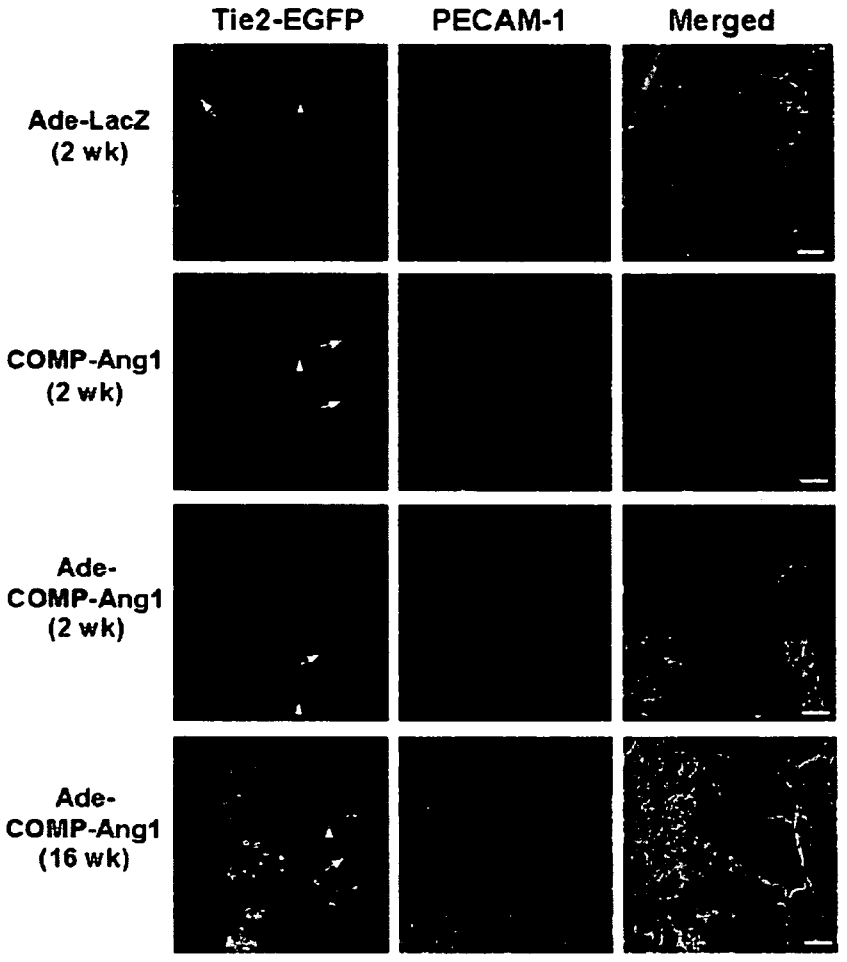

Figure 6. Induction of Tie2 expression in COMP-Ang1–induced vascular remodeling. Tie2-GFP transgenic mice (10 weeks old) were treated with daily injection of 200 μg of COMP-Ang1 recombinant protein (COMP-Ang1) for 2 weeks or a single injection of 1×10^9 pfu Ade-LacZ or Ade-COMP-Ang1. At 2 and 16 weeks after the beginning of the treatments, Tie2 expression in tracheal vessels was visualized by GFP expression (green) and PECAM-1 immunostaining (red), and the images were merged. The results from 4 experiments were similar. Arrowhead indicates terminal arterioles; arrow, precapillary arterioles. Scale bar=50 μm.

nal arterioles in mouse trachea. Therefore, we examined the extent of Tie2 expression using transgenic mice with Tie2 promoter–driven green fluorescent protein (GFP).[12] In the tracheal mucosa of adult mice, Tie2 expression was not detectable in most endothelial cells of postcapillary venules, whereas it was moderately expressed in endothelial cells of terminal and precapillary arterioles of tracheal vessels (Figure 6). Thus, differential enlargement of tracheal vessels on COMP-Ang1 stimulation is not dependent on the extent of Tie2 expression. However, Tie2 expression was markedly increased in endothelial cells of collecting venules, venules, postcapillary venules, and capillaries at 2 weeks after the Ade-COMP-Ang1 treatment (Figure 6), which is somewhat consistent with a recent report with Ade-Ang1.[8] Tie2 expression was further increased in endothelial cells of the same vessels at 16 weeks after the Ade-COMP-Ang1 treatment (Figure 6). In contrast, Tie2 expression was not changed in any endothelial cells of enlarged tracheal vessels at 2 weeks after the recombinant COMP-Ang1 protein treatment (Figure 6). Area densities of Tie2 expression in a given microscopic field area (0.22 mm^2) for arterioles, capillaries, and venules in tracheal mucosa were 8.2±1.7, 2.8±0.4, and 3.3±0.6% (mean±SD from 4 mice), respectively, after Ade-LacZ treatment (at 2 weeks); 7.6±1.9, 3.1±0.5, and 3.7±0.6% after COMP-Ang1 protein treatment (at 2 weeks); 11.3±2.2, 10.3±1.7, and 28.1±5.4% after Ade-COMP treatment (at 2 weeks); and 13.3±2.7, 18.2±3.5, and 47.7±7.2 after Ade-COMP treatment (at 16 weeks). In addition, Tie2 expression was notably higher in the enlarged veins of abdominal skin and the sinusoidal capillaries in liver of the mice treated with Ade-COMP-Ang1 than the mice treated with Ade-LacZ at 16 weeks after the treatment (online Figure II). Thus, Tie2 expression in venular and capillary endothelial cells could be induced with long-term and sustained Tie2 stimulation induced by Ade-COMP-Ang1 but not with short-term spiked Tie2 stimulation induced by recombinant COMP-Ang1 protein.

COMP-Ang1–Induced Vascular Enlargement Could Result From Circumferential Endothelial Cell Proliferation

COMP-Ang1–induced enlargement of blood venules appears to result from endothelial cell proliferation rather than vasodilation or endothelial cell hypertrophy because the endothelial cells were normal in size (Figure 7A and 7B). To test this possibility, we examined by immunostaining the number of endothelial cells positive for phosphohistone H3 (nuclear protein of diving cell). Numerous phosphohistone H3–positive immunostained endothelial cells were detected in various portions including postcapillary venules, capillaries, collect-

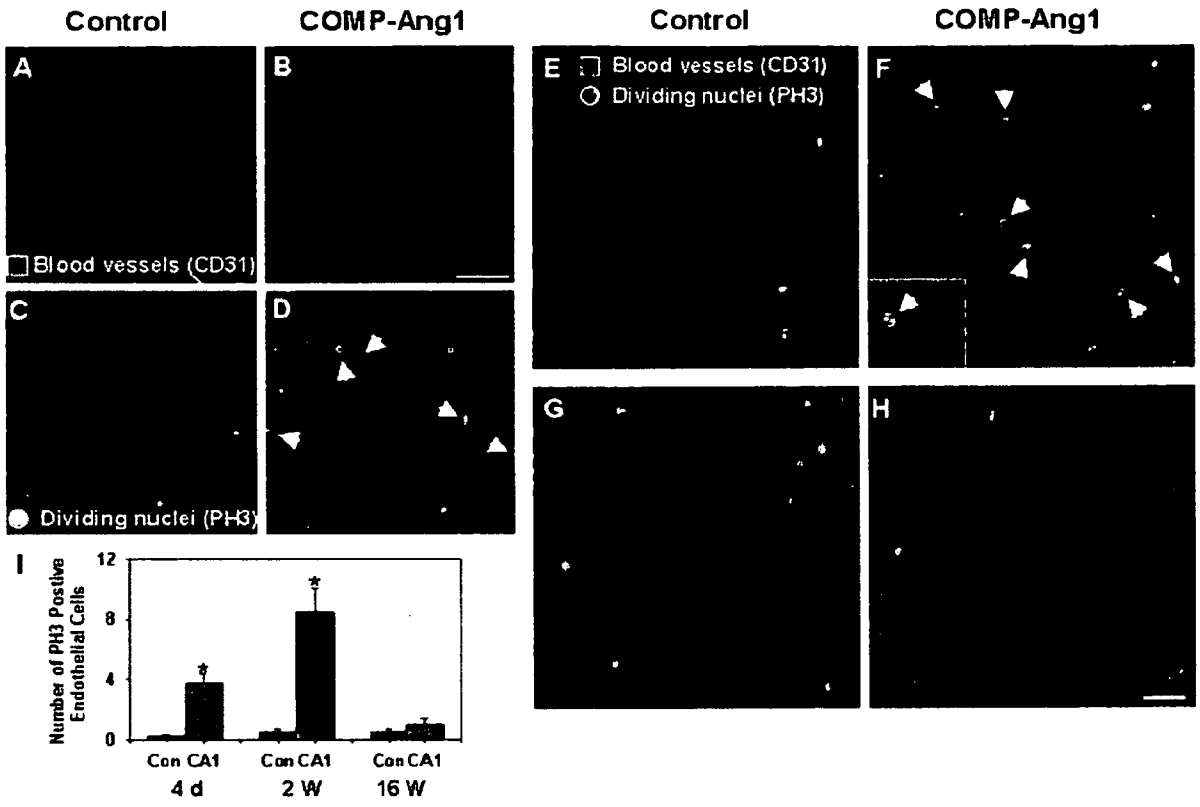

Figure 7. Increased number of dividing endothelial cells during COMP-Ang1–induced enlargement. FVB/N mice were treated with 1×10^9 pfu Ade-LacZ (control; A, C, E, and G) or Ade-COMP-Ang1 (COMP-Ang1; B, D, F, and H). Four days (C and D), 2 weeks (E and F), and 16 weeks (G and H) later, tracheal vessels were visualized with PECAM-1 (CD31) immunostaining (red) and phosphohistone H3 (PH3) immunostaining (green). F, Arrow indicates PH3-immunopositive endothelial cells; white square, PH3-immunopositive endothelial cells in postcapillary venule at higher magnification. Scale bar 50 μm. I, Number of PH3-immunopositive endothelial cells in a given 0.21 mm^2 area. Bars represent mean±SD from 4 mice. Con indicates control; CA1, COMP-Ang1. *$P<0.05$ vs Con.

ing venules, venules, and terminal arterioles of tracheal vessels at 4 days and 2 weeks after the Ade-COMP-Ang1 treatment (Figure 7D, 7F, and 7I) or after recombinant COMP-Ang1 protein treatment (data not shown). However, almost no phosphohistone H3–positive endothelial cells were detected in any portion of tracheal vessels at 4 days or 2 and 16 weeks after the Ade-LacZ treatment and at 16 weeks after the Ade-COMP-Ang1 treatment (Figure 7C, 7E, 7G, and 7I). These findings indicate that vascular enlargement induced by COMP-Ang1 is more likely to result from endothelial cell proliferation depending on concentration of circulating COMP-Ang1 than from vasodilation or endothelial cell hypertrophy.

COMP-Ang1–Induced Postcapillary Venule Enlargement Is Not Accompanied by Pericyte Recruitment

Ang1 is known to be a strong growth factor for pericyte recruitment to nascent endothelial cells during vasculogenesis in physiological and pathological conditions.[3–5] Therefore, we examined the interaction between endothelial cells and pericytes in the enlarged blood vessels of the trachea by double-immunostaining for endothelial cells and pericytes at 4 weeks after Ade-LacZ or Ade-COMP-Ang1 treatment. The interaction of endothelial cells and pericytes in most of tracheal blood vessels (except postcapillary venules) in mice that received Ade-COMP-Ang1 was similar to that in mice that received Ade-LacZ (Figure 8). Although less interaction of endothelial cells with pericytes was found on the enlarged postcapillary venules than elsewhere, the number of pericytes of the enlarged postcapillary venules was similar to the control postcapillary venules (Figure 8). Thus, COMP-Ang1 did not promote pericyte recruitment to the COMP-Ang1–induced enlarged venules in the trachea.

Discussion

The most important and novel finding in this study is that enlargement of tracheal blood vessels and enhancement of tracheal tissue blood flow induced by long-term and sustained exposure to COMP-Ang1 had not regressed for up to 16 weeks, despite the fact that exposure to COMP-Ang1 had already been discontinued at 6 to 7 weeks in adult mice. In comparison, enlargement of tracheal blood vessels induced by short-term intermittent exposure to COMP-Ang1 regressed on discontinuation of recombinant COMP-Ang1 treatment. Therefore, long-lasting vascular enlargement and enhancement of blood flow can be achieved by long-term and sustained exposure to COMP-Ang1.

Like other therapeutic proteins, circulating COMP-Ang1 rapidly disappeared in the plasma, probably because of its trapping by the Tie2 receptor of lung endothelial cells.[15]

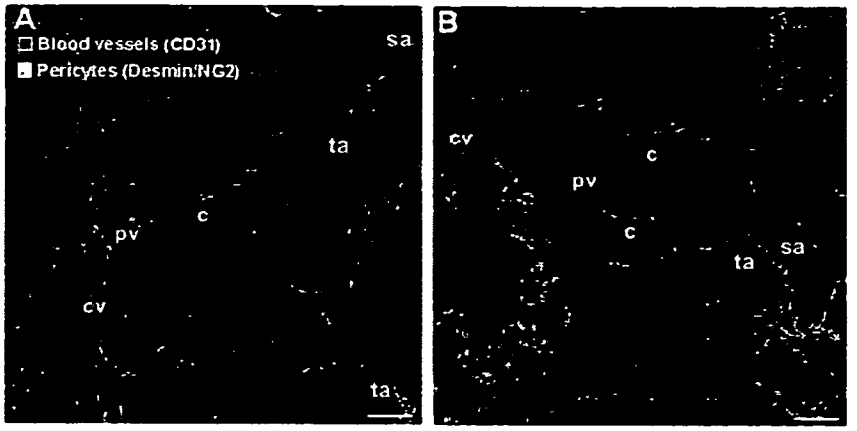

Figure 8. Interaction between endothelial cells and pericytes in COMP-Ang1–induced enlarged tracheal vessels. FVB/n mice were treated with 1×10^9 pfu Ade-COMP-Ang1 (B) or Ade-LacZ (A). Four weeks later, tracheal vessels were visualized with PECAM-1 (CD31) immunostaining (red), and pericytes were visualized with desmin/NG2 immunostaining (green). The results from 4 experiments were similar. Scale bar=50 μm.

However, we were able to achieve long-term (>4 weeks) and sustained (>1000 ng/mL) circulating COMP-Ang1 in mice by a single intravenous injection of 1×10^9 pfu Ade-COMP-Ang1. Throughout these experiments, we learned that long-term (≈6 weeks) and sustained exposure to COMP-Ang1 produced long-lasting enlargement of postcapillary venules and terminal arterioles in the tracheal mucosa, whereas short-term (≈2 weeks) and intermittent exposure to COMP-Ang1 produced reversible enlargements of these vessels. Similar to our results, another study found that long-term (4 weeks) sustained exposure to vascular endothelial growth factor (VEGF) produced long-lasting acquired vascular remodeling in liver, whereas short-term (2 weeks) sustained exposure to VEGF produced reversible vascular remodeling.[16] What are the major mechanisms and factors that produce long-lasting and reversible vascular remodeling? Is there a threshold stimulation of Tie2 by COMP-Ang1 that can produce permanent enlargement? Our results suggest that auto-amplification of Tie2 expression by treatment with COMP-Ang1 above a certain dose and exposure period could be one of the mechanisms. Once Tie2 expression is activated by a long-term and excess exposure to COMP-Ang1, after discontinuation of COMP-Ang1, the subsequent activation of Tie2 might be achieved by endogenous circulating Ang1 or increased shear stress caused by increased blood flow.[17] However, auto-amplification of Tie2 expression cannot be achieved below a certain dose and exposure period of COMP-Ang1, as evidenced by the experiments with intravenous administration of COMP-Ang1 recombinant protein. Therefore, the dose and the exposure period of COMP-Ang1 or VEGF should be considered in any therapeutic approaches where permanent vascular enlargements are needed to alleviate dysfunctions of ischemic tissues.

Tie1, an endothelial-specific receptor tyrosine kinase, shares a high degree of homology with Tie2. Although Tie1 was isolated more than a decade ago,[18] no ligand had been found to activate it. Recently, Saharinen et al demonstrated that COMP-Ang1 stimulated Tie1 phosphorylation in cultured endothelial cells.[19] Moreover, they showed that COMP-Ang1–induced Tie1 activation was amplified via Tie2 and was more efficient than native Ang1- and Ang4-induced Tie1 activation. Thus, COMP-Ang1 and Ang1 are now known to be activating ligands for both Tie1 and Tie2. However, our data indicate that COMP-Ang1–induced vascular remodeling in adult tracheal vessels is mainly mediated through activation of Tie2, not by Tie1. (See expanded Discussion section in the online data supplement.)

Although Ang1 induces vascular enlargement and has therapeutic benefits to ischemic tissues in several experimental animal models,[6,7,9] little is known about whether the vascular enlargement is accompanied by enhanced blood flow. Our results showed that COMP-Ang1–induced vascular enlargement was accompanied by enhanced tissue blood flow in the trachea. Therefore, enhanced blood flow through arteriolar and venular enlargements induced by COMP-Ang1 could provide a great therapeutic benefit to ischemic peripheral tissues. In fact, Ang1-induced vessel enlargement is a unique characteristic among many growth factors. Our immunohistological examination of phosphohistone H3 revealed that COMP-Ang1–induced vascular enlargements were evidently the result of endothelial proliferation, which is consistent with a recent report.[14] Thus, arteriolar and venular enlargements are achieved mainly by circumferential endothelial proliferation, which is a unique phenomenon and is different from multidirectional endothelial cell proliferation during vasculogenesis and angiogenesis. Moreover, our results revealed that different organs showed different sensitivities to long-term and sustained COMP-Ang1. In fact, blood vessels in the skin, heart, adrenal cortex, and liver, among other organs, are relatively sensitive to the COMP-Ang1–induced vascular enlargement. Therefore, COMP-Ang1 could provide a great therapeutic benefit to patients with delayed skin wound healing and ischemic heart diseases through its ability to promote vascular remodeling. Nevertheless, the mice treated with long-lasting and sustained COMP-Ang1 did not show any significant changes in body weight, systemic blood pressure, or heart rate. More detailed analysis will be necessary to clarify how it is possible that the mice with enlarged blood vessels caused by long-term and sustained COMP-Ang1 have normal blood pressure and heart rate.

Ang1 is known to be a strong growth factor for pericyte recruitment to nascent endothelial cells during development.[3–5] This Ang1-induced pericyte recruitment is related to the Ang1-induced antileakage effect on VEGF and proinflammatory stimuli.[5] However, our results show a lower number and poorer covering of pericytes in COMP-Ang1–

induced enlarged postcapillary venules. In fact, in a mouse model that completely blocks pericyte recruitment to developing vessels by injection of antagonistic monoclonal antibody against platelet-derived growth factor receptor-β, Angl is able to restore a hierarchical architecture of growing blood vessels and rescues retinal edema and hemorrhage even in the absence of pericyte recruitment.[20] Thus, COMP-Angl may be able to assemble endothelial cells in a frame of hierarchical architecture without pericyte recruitment in the COMP-Angl–induced enlarged blood vessels.

In conclusion, long-lasting vascular enlargement and enhancement of blood flow can be achieved by long-term and sustained exposure to COMP-Angl.

Acknowledgments

Supported, in part, by the Bio-Challenge Program and the National Research Laboratory Program (2004-02376 to G.Y.K.) of the Korean Ministry of Science and Technology, the Korea Health R&D Project (0405-DB01-0104-0006 to G.Y.K.), the Ministry of Health & Welfare, and the Korea Science and Engineering Foundation (R01-2004-000-10045-0 to B.H.J.). Also supported by National Institutes of Health grants HL-24136 and HL-59157 from the National Heart, Lung and Blood Institute (to D.M.D.).

References

1. Davis S, Aldrich TH, Jones PF, Acheson A, Compton DL, Jain V, Ryan TE, Bruno J, Radziejewski C, Maisonpierre PC, Yancopoulos GD. Isolation of angiopoietin-1, a ligand for the TIE2 receptor by secretion-trap expression cloning. *Cell*. 1996;87:1161–1169.
2. Dumont DJ, Gradwohl G, Fong GH, Puri MC, Gertsenstein M, Auerbach A, Breitman ML. Dominant-negative and targeted null mutations in the endothelial receptor tyrosine kinase, tek, reveal a critical role in vasculogenesis of the embryo. *Genes Dev*. 1994;8:1897–1909.
3. Suri C, Jones PF, Patan S, Bartunkova S, Maisonpierre PC, Davis S, Sato TN, Yancopoulos GD. Requisite role of angiopoietin-1, a ligand for the TIE2 receptor, during embryonic angiogenesis. *Cell*. 1996;87:1171–1180.
4. Suri C, McClain J, Thurston G, McDonald DM, Zhou H, Oldmixon EH, Sato TN, Yancopoulos GD. Increased vascularization in mice overexpressing angiopoietin-1. *Science*. 1998;282:468–471.
5. Thurston G, Suri C, Smith K, McClain J, Sato TN, Yancopoulos GD, McDonald DM. Leakage-resistant blood vessels in mice transgenically overexpressing angiopoietin-1. *Science*. 1999;286:2511–2514.
6. Shyu KG, Manor O, Magner M, Yancopoulos GD, Isner JM. Direct intramuscular injection of plasmid DNA encoding angiopoietin-1 but not angiopoietin-2 augments revascularization in the rabbit ischemic hindlimb. *Circulation*. 1998;98:2081–2087.
7. Chae JK, Kim J, Lim ST, Chung MJ, Kim WH, Kim HG, Ko JK, Koh GY. Co-administration of angiopoietin-1 and vascular endothelial growth factor enhances collateral vascularization. *Arterioscler Thromb Vasc Biol*. 2000;20:2573–2578.
8. Baffert F, Thurston G, Rochon-Duck M, Le T, Brekken R, McDonald DM. Age-related changes in vascular endothelial growth factor dependency and angiopoietin-1-induced plasticity of adult blood vessels. *Circ Res*. 2004;94:984–992.
9. Zhou YF, Stabile E, Walker J, Shou M, Baffour R, Yu Z, Rott D, Yancopoulos GD, Rudge JS, Epstein SE. Effects of gene delivery on collateral development in chronic hypoperfusion: diverse effects of angiopoietin-1 versus vascular endothelial growth factor. *J Am Coll Cardiol*. 2004;44:897–903.
10. Cho CH, Kammerer RA, Lee HJ, Steinmetz MO, Ryu YS, Lee SH, Yasunaga K, Kim KT, Kim I, Choi HH, Kim W, Kim SH, Park SK, Lee GH, Koh GY. COMP-Angl: a designed angiopoietin-1 variant with nonleaky angiogenic activity. *Proc Natl Acad Sci U S A*. 2004;101:5547–5552.
11. Hwang SJ, Choi HH, Kim KT, Hong HJ, Koh GY, Lee GM. Expression and purification of recombinant human angiopoietin-2 produced in CHO cells. *Protein Express Purif*. 2005;39:175–183.
12. Schlaeger TM, Bartunkova S, Lawitts JA, Teichmann G, Risau W, Deutsch U, Sato TN. Uniform vascular-endothelial-cell-specific gene expression in both embryonic and adult transgenic mice. *Proc Natl Acad Sci U S A*. 1997;94:3058–3063.
13. Baluk P, Raymond WW, Ator E, Coussens LM, McDonald DM, Caughey GH. Matrix metalloproteinase-2 and -9 expression increases in Mycoplasma-infected airways but is not required for microvascular remodeling. *Am J Physiol Lung Cell Mol Physiol*. 2004;287:L307–L317.
14. McDonald DM. Endothelial gaps and permeability of venules in rat tracheas exposed to inflammatory stimuli. *Am J Physiol*. 1994;266:L61–L83.
15. Cho CH, Kammerer RA, Lee HJ, Yasunaga K, Kim KT, Choi HH, Kim W, Kim SH, Park SK, Lee GM. A designed angiopoietin-1 variant, COMP-Angl, protects against radiation-induced endothelial cell apoptosis. *Proc Natl Acad Sci U S A*. 2004;101:5553–5558.
16. Dor Y, Djonov V, Abramovitch R, Itin A, Fishman GI, Carmeliet P, Goelman G, Keshet E. Conditional switching of VEGF provides new insights into adult neovascularization and pro-angiogenic therapy. *EMBO J*. 2002;21:1939–1947.
17. Lee HJ, Koh GY. Shear stress activates Tie2 receptor tyrosine kinase in human endothelial cells. *Biochem Biophys Res Commun*. 2003;304:399–404.
18. Partanen J, Armstrong E, Makela TP, Korhonen J, Sandberg M, Renkonen R, Knuutila S, Huebner K, Alitalo K. A novel endothelial cell surface receptor tyrosine kinase with extracellular epidermal growth factor homology domains. *Mol Cell Biol*. 1992;12:1698–1707.
19. Saharinen P, Kerkela K, Ekman N, Marron M, Brindle N, Lee GM, Augustin H, Koh GY, Alitalo K. Multiple angiopoietin recombinant proteins activate the Tie1 receptor tyrosine kinase and promote its interaction with Tie2. *J Cell Biol*. 2005;169:239–243.
20. Uemura A, Ogawa M, Hirashima M, Fujiwara T, Koyama S, Takagi H, Honda Y, Wiegand SJ, Yancopoulos GD, Nishikawa S. Recombinant angiopoietin-1 restores higher-order architecture of growing blood vessels in mice in the absence of mural cells. *J Clin Invest*. 2002;110:1619–1628.

Enhanced Functional Gap Junction Neoformation by Protein Kinase A–Dependent and Epac-Dependent Signals Downstream of cAMP in Cardiac Myocytes

Satoshi Somekawa, Shigetomo Fukuhara, Yoshikazu Nakaoka, Hisakazu Fujita, Yoshihiko Saito, Naoki Mochizuki

Abstract—Gap junctions (GJs) constituted by neighboring cardiac myocytes are essential for gating ions and small molecules to coordinate cardiac contractions. cAMP is suggested to be a potent stimulus for enhancement of GJ function. However, it remains elusive how cAMP potentiates the GJ of cardiomyocytes. Here we demonstrated that the gating function of GJ is enhanced by the protein kinase A (PKA)–dependent signal, and that the accumulation of connexin43 (Cx43), the most abundant Cx in myocytes, is enhanced by an exchange protein directly activated by cAMP (Epac) (Rap1 activator)–dependent signal. The gating function of GJs was analyzed by microinjected dye transfer method. The accumulation of Cx43 was analyzed by quantitative immunostaining. Using the PKA-specific activator N^6-benzoyladenosine-3′,5′-cyclic monophosphate (6Bnz) and Epac-specific activator 8-(4-chlorophenylthio)-2′-*O*-methyladenosine-3′,5′-cyclic monophosphate (8CPT), we could delineate the two important downstream signals of cAMP for enhanced GJ neoformation. Whereas 6Bnz potentiated gating function of GJs with slight accumulation of Cx43 at cell–cell contacts, 8CPT remarkably enhanced the accumulation of Cx43 with a slight effect on gating. We further noticed that adherens junctions (AJs) were maturated by 8CPT, as marked by increased neural-cadherin immunostaining. Because AJ formation precedes the GJ formation, AJ formation accelerated by Epac-Rap1 signal may result in enhanced GJ formation. The involvement of Epac-Rap1 signal in GJ neoformation was further confirmed by evidence that inactivation of Rap1 by overexpression of Rap1GAP1b perturbed the accumulation of Cx43 at cell–cell contacts. Collectively, PKA and Epac cooperatively enhance functional GJ neoformation in cardiomyocytes. (***Circ Res.* 2005;97:655-662.**)

Key Words: gap junction ■ connexin43 ■ myocardial structure ■ cardiac gap junction connexins

Gap junctions (GJs) are channels formed by two docking connexons; one connexon is provided by each of the two contiguous cells and is constituted of six connexin (Cx) molecules.[1] Among the 20 Cx members, Cx40, Cx43, and Cx45 are expressed in the heart.[2] Of the three, Cx43 is predominantly expressed in working heart muscle cells.[3,4] GJs in the heart are characterized by their localization at the intercalated disk between each myocyte and also by their role in electrical conductance required for coordinated electrical excitation.[5] Myocytes electrically coupled by GJs show synchronized contraction. The importance of Cx43 in electrical excitation in vivo is evident by cardiac-specific depletion of Cx43 leading to cardiac arrhythmia.[6]

The overall function of GJs depends on the number of GJs and the gating function of assembled GJs. GJs are upregulated by increased transcription of Cx, increased distribution of Cx at cell–cell contacts, and decreased degradation of Cx from the cell membrane. cAMP increases Cx43 mRNA.[7] cAMP also enhances the trafficking of Cx43 from the endoplasmic reticulum/Golgi apparatus to the plasma membrane.[8] Cx43 turnover is regulated by proteosomal and lysosomal degradation, and the half-life of Cx43 is less than two hours, suggesting that a rapid synthesis and trafficking system operates in cardiac myocytes.[9]

GJ is modulated by the phosphorylation of Cx43 on Ser and Tyr residues. The intercellular communication through Cx43 is decelerated and accelerated by its phosphorylation on Ser368 by protein kinase C and on Ser364 by protein kinase A (PKA), respectively.[10,11] In addition to Ser phosphorylation, phosphorylated Cx43 on Tyr247 and Tyr265 is repressed from junctional communication.[12] In addition to phosphorylation, GJ formation is regulated by Cx43-binding molecules. Cx43 binds to the junctional adhesion molecule-associating proteins zonula occludens-1 (ZO-1) and β-catenin.[13,14] Dominant-negative ZO-1, which dissociates the endogenous ZO-1 from Cx43, disturbs the localization of

Original received May 10, 2005; resubmission received July 12, 2005; revised resubmission received August 11, 2005; accepted August 16, 2005.
From the Department of Structural Analysis (S.F., Y.N., H.F., N.M.), National Cardiovascular Center Research Institute, Suita, Osaka; the First Department of Internal Medicine (S.S., Y.S.), Nara Medical University, Kashihara, Nara, Japan.
Correspondence to Naoki Mochizuki, Department of Structural Analysis, National Cardiovascular Center Research Institute, 5-7-1 Fujishirodai, Suita, Osaka 565-8565, Japan. E-mail nmochizu@ri.ncvc.go.jp
© 2005 American Heart Association, Inc.

Circulation Research is available at http://circres.ahajournals.org DOI: 10.1161/01.RES.0000183880.49270.f9

Cx43 at the cell–cell contacts, resulting in the reduced conductance of GJs.[13] Wnt-1 signal prevents β-catenin degradation, thereby increasing β-catenin, which not only drives Cx43 expression but also associates with the Cx43 at the cell–cell contacts, where β-catenin localizes with cadherin.[14]

cAMP-induced Cx43 assembly has been extensively characterized in terms of Cx43 synthesis, delivery to the plasma membrane, and phosphorylation, which is believed to depend exclusively on PKA.[15] However, other downstream molecules of cAMP have not been elucidated in the neoformation of GJs. We and others have demonstrated that exchange protein directly activated by cAMP (Epac)/cAMP-GEF, a guanine nucleotide exchange factor (GEF) for Rap1, is activated by cAMP,[16,17] and that cAMP–Epac-Rap1 signal enhances the barrier function of vascular endothelial cells by stabilizing cadherin-mediated cell adhesion.[18,19] Analogous to this Epac-induced cadherin-based cell adhesion, we hypothesized that Epac may be involved in GJ neoformation as a cAMP-triggered signaling molecule in cardiac myocytes.

In this study, we investigated the molecular mechanism by which GJ neoformation is regulated by cAMP using a PKA-specific activator and an Epac-specific activator. We analyzed the GJ accumulation at cell–cell contacts by immunostaining of Cx43 and the gating function of GJs by dye spreading in neonatal rat cardiomyocytes (NRCMs) stimulated with these activators. We demonstrate that the Cx43 accumulation at cell–cell contacts depends on Epac and that dye spreading depends on PKA. Therefore, PKA and Epac downstream of cAMP cooperatively enhance functional GJ neoformation in cardiac myocytes.

Materials and Methods

Reagents and cAMP Analogs

Dibutyryl-cAMP (dbcAMP) was purchased from Sigma-Aldrich, Epac-specific activator 8-(4-chlorophenylthio)-2′-*O*-methyladenosine-3′,5′-cyclic monophosphate (8CPT) from Calbiochem; and PKA-specific activator N^6-benzoyladenosine-3′,5′-cyclic monophosphate (6Bnz) was from BIOLOG Life Science Institute. Other chemical compounds, antibodies, and adenoviruses are listed in the supplemental information (available online at http://circres.ahajournals.org).

Cell Culture

NRCMs were isolated from Wistar rats (1 to 2 days old; Kiwa Jikken Dobutsu, Japan) on a Percoll gradient as described previously.[20] The details of cardiac myocyte preparation are described in the supplemental information. The NRCMs spread onto the glass-base dishes for 24 hours after isolation were subjected to immunostaining or dye transfer assay after drug treatment for another 12 hours. We observed that the adherens junctions (AJs) were not maturated, although NRCMs contacted each other before the drug treatment, indicating that we used the reassembling NRCMs for the experiments. Experiments using animals were approved by our institutional animal use and care committee. All animal procedures were performed according to the *Guide for the Care and Use of Laboratory Animals* (NIH, revision 1996).

Immunocytochemistry

NRCMs stimulated with cAMP analogs were immunostained as described previously.[21] Briefly, cells cultured on glass-base dish were blocked with PBS containing 4% BSA for 1 hour at room temperature (RT), then stained with anti-Cx43, anti–sarcomeric α-actinin (S-αA), and anti–neural (N)-cadherin at RT. Protein reacting with primary antibodies was visualized with Alexa 488–labeled goat anti-rabbit IgG and Alexa 546–labeled goat anti-mouse IgG. Images were recorded with a confocal microscope (BX50WI; Olympus). For quantitative immunofluorescence analysis, images were also recorded using an epifluorescence microscope (IX-71; Olympus) controlled by MetaMorph version 6.2 software (Molecular Devices). The number of Cx43-positive dots at the cell–cell contacts on the fluorescence images were counted as Cx43 puncta.

Gating Function of GJs Analyzed by Microinjected Dye Transfer

Microinjected dye transfer was performed as described by Doble et al, with minor modifications.[22] The details of dye transfer method are described in the supplemental information.

RT-PCR Analysis

Total RNAs extracted from NRCMs and human cervical carcinoma cell line (HeLa) cells using Trizol (Invitrogen) were reverse-transcribed using SuperScript II and random primers (Invitrogen). The resultant DNAs were PCR-amplified using Epac-specific primers described in the supplemental information.

Western Blot Analysis and N-Cadherin Translocation Assay

NRCMs were lysed in buffer described in the supplemental information. Lysates precleared by centrifugation at 15 000*g* for 10 minutes were subjected to SDS-PAGE and immunoblotting with antibodies as indicated in Figures 3, 4, 5, and 6. Proteins reacting with primary antibodies were visualized by an enhanced chemiluminescence system (Amersham Biosciences) with peroxidase-conjugated and species-matched secondary antibodies and analyzed with an LAS-1000 system (Fuji Film). N-cadherin translocation assay was performed as described previously.[18]

Detection of GTP-Bound Form of Rap1

Rap1 activity was assessed by a modified Bos method as described previously.[23] Briefly, NRCMs starved in DMEM for 3 hours were treated with the stimulants as indicated in Figures 3 and 6 and lysed at 4°C in a pull-down lysis buffer described in the supplemental information. GTP-bound Rap1 was collected on glutathione *S*-transferase fused with Rap1 binding domain of Ral guanine nucleotide dissociation stimulator precoupled to glutathione-Sepharose beads and subjected to SDS-PAGE followed by immunoblotting using anti-Rap1.

Statistical Analysis

The results were expressed as the mean±SD. Student *t* test was used to analyze differences between two groups. Group differences were assessed with one-way ANOVA or two-way ANOVA, followed by post hoc comparisons tested with Scheffe's method. At least 3 fields randomly selected from each culture for analysis of Cx43 staining or at least 4 cells for dye transfer assay from each culture were used to yield a single value for each culture. The number of the cultures for analysis was indicated in the figure legends as n. Significant differences were indicated as P value <0.05 (*).

Results

cAMP Enhances Functional GJ Neoformation in Cultured NRCMs

Because cAMP has been reported previously to enhance GJ formation,[7] we confirmed the dbcAMP–regulated functional GJ neoformation by quantitatively analyzing Cx43 accumulation at the cell–cell contacts by immunostaining and gating function of GJs by microinjected dye transfer assay. dbcAMP enhanced the Cx43 accumulation at the cell–cell contacts (Figure 1A and 1B). To neglect the possibility of cardiac fibroblast contamination in the NRCMs in the following

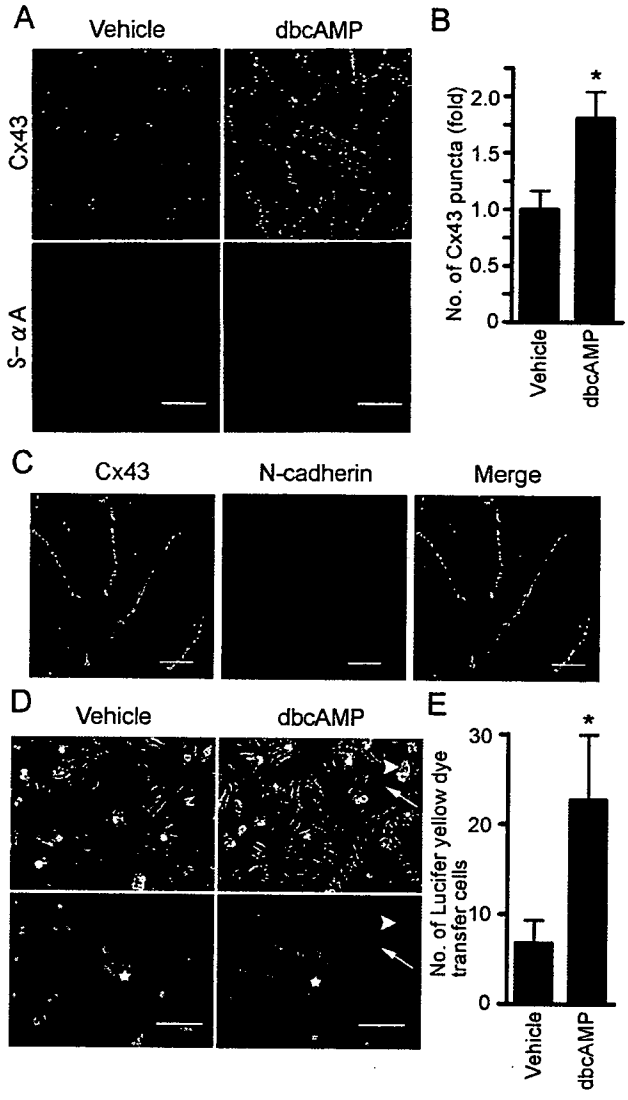

Figure 1. cAMP induces Cx43 accumulation at cell–cell contacts and enhances gap junctional intercellular communication. A, NRCMs cultured 24 hours after cell preparation were stimulated with vehicle or 1 mmol/L dbcAMP for 12 hours. Cells were stained with anti-Cx43 (green) and anti-S-αA (red). Images were obtained through a confocal microscope (BX50WI). Bar=20 μm. B, NRCMs stimulated by dbcAMP were analyzed for Cx43 accumulation by counting the number of puncta at cell–cell contacts. Mean number±SD is expressed as fold increase relative to that observed in the cell treated with vehicle. *$P<0.05$ vs vehicle as analyzed by Student's t test (n=4). Three fields randomly selected from each culture were used for measuring the fold activation between vehicle- and dbcAMP-treated culture by counting Cx43-positive puncta. C, Cells treated with dbcAMP were immunostained with anti-Cx43 (green) and anti-N-cadherin (red). A merged image is shown on the right. Note that puncta for Cx43 are localized to cell–cell contacts as indicated by the N-cadherin immunostaining. Bar=5 μm. D, Microinjected dye transfer assay shows the extent of dye transferring between neighboring cells through GJs. NRCMs stimulated with 1 mmol/L dbcAMP for 12 hours were microinjected with 10% Lucifer yellow. Cells 3 minutes after dye injection were phase contrast imaged (top panels) and fluorescence imaged (bottom panels). Asterisks indicate dye-injected cells. Arrows and arrowheads denote typical dye-transferred cell and cell debris emitting nonspecific fluorescence, respectively. Bar=50 μm. E, Quantitative analysis of D is shown as mean number of dye-positive cells in either vehicle or dbcAMP-treated NRCMs. *$P<0.05$ as analyzed by Student's t test (n=6).

experiments, and to show the confluence of the NRCMs, cells were immunostained for sarcomeric α-actinin (Figure 1A, bottom). The Cx43 puncta in the cells treated with dbcAMP for 12 hours were clearly observed at the cell–cell contacts, where N-cadherin localized (Figure 1C), indicating that dbcAMP induces the accumulation of Cx43 at the cell–cell contacts. We investigated the effect of dbcAMP on gating function of GJs by microinjected dye transfer assays (Figure 1D and 1E). Microinjected dye was more widely transferred to the neighboring cells in dbcAMP-treated NRCMs than vehicle-treated cells (Figure 1D). The quantitative data are shown in Figure 1E. These results are in agreement with previous reports[7,8] and validated the assays we used in this study.

PKA Is Required But Not Sufficient Alone for cAMP-Enhanced GJ Neoformation

Because PKA is involved in the enhancement of GJ formation,[15] we first tested the effect of H89, a specific PKA inhibitor, on cAMP-enhanced accumulation of Cx43. Unexpectedly, H89 did not block the dbcAMP-induced accumulation of Cx43 (Figure 2A and 2B), although H89 did block cAMP-enhanced intercellular communication assessed by microinjected dye transfer assays (Figure 2C).

We next examined the effect of 6Bnz, a specific activator for PKA,[24] on intercellular communication and Cx43 accumulation at cell–cell contacts to directly assess the involvement of PKA in cAMP-enhanced GJ formation. 6Bnz induced Cx43 accumulation slightly but to a much lesser extent than dbcAMP (Figure 2D and 2E). Notably, 6Bnz enhanced dye transfer to a greater extent than vehicle but to a lesser extent than dbcAMP (Figure 2F). These results indicate that PKA signaling is required but not sufficient alone for cAMP-enhanced GJ neoformation and suggest that there is a novel signaling downstream of cAMP in addition to PKA involved in Cx43 accumulation at cell–cell contacts for functional GJ neoformation.

cAMP Activates PKA and Epac-Rap1 Signaling in NRCMs

Epac has been identified as a novel cAMP target and a Rap1-specific GEF. We therefore hypothesized that Epac-Rap1 signaling may be involved in cAMP-enhanced GJ neoformation. RT-PCR analysis revealed the expression of Epac in NRCM but not in HeLa cells used as a negative control (Figure 3A). To test the hypothesis, we first examined whether dbcAMP induces the activation of Rap1 and the phosphorylation of cAMP response element binding protein (CREB) in NRCMs. As shown in Figure 3B, dbcAMP induced Rap1 and CREB activation in NRCMs. Rap1 activation by dbcAMP is dependent on time and concentration (supplemental Figure IA and IB, available online at http://circres.ahajournals.org). H89 inhibited dbcAMP-induced CREB phosphorylation but not dbcAMP-induced Rap1 activation (Figure 3B and 3C), indicating that Rap1 activation does not depend on PKA, whereas CREB phosphorylation depends exclusively on PKA. We next tested whether Rap1 activation and CREB phosphorylation are induced by 8CPT, which has been developed recently as a specific activator for Epac.[25] 8CPT only activated Rap1, not CREB. In striking contrast, 6Bnz induced CREB activation but did not affect

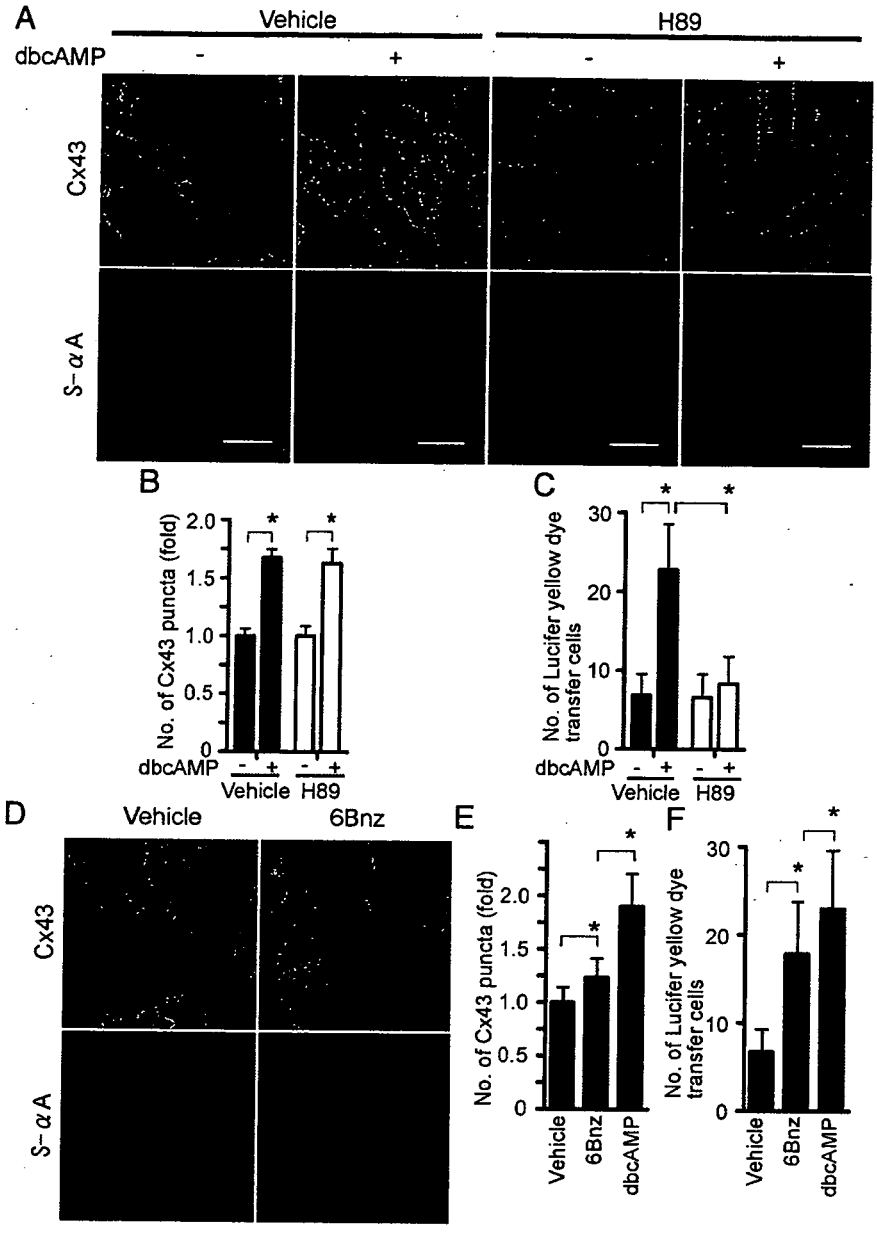

Figure 2. PKA signaling mainly contributes to gating function of GJs. A, NRCMs pretreated with or without 5 μmol/L H89 for 30 minutes were stimulated with or without 1 mmol/L dbcAMP in the presence or absence of 5 μmol/L H89 for 12 hours. After the stimulation, cells were immunostained with anti-Cx43 and anti-S-αA as described in Figure 1A legend. Bar=20 μm. B, Cx43 accumulation in cells treated as in A was quantitatively analyzed. Statistical significance between groups was analyzed by two-way ANOVA with Scheffe's method, indicating that the factor of with/without dbcAMP is significant but not that of vehicle/H89 (*P<0.05; n=6) C, Effect of H89 on dbcAMP-enhanced gap junctional intercellular communication was evaluated by microinjected dye transfer assay as described in Figure 1E legend. Statistical significance between groups was analyzed by two-way ANOVA with Scheffe's method, indicating that both factors, with/without dbcAMP and vehicle/H89, are significant (*P<0.05; n=6). D, NRCMs were stimulated with either vehicle or 1 mmol/L 6Bnz for 12 hours and immunostained with anti-Cx43 and anti-S-αA. Bar=20 μm. E, The effect of 1 mmol/L 6Bnz on Cx43 accumulation at the cell–cell contacts was evaluated similarly to Figure 1B. Statistical significance between groups was analyzed by one-way ANOVA with Scheffe's method (*P<0.05; n=4). F, The effect of 6Bnz on junctional intercellular communication between NRCMs was similarly evaluated by microinjected dye transfer assay to the Figure 1D. Statistical significance was evaluated by one-way ANOVA with Scheffe's method (*P<0.05; n=4).

Rap1 activity (Figure 3D and 3E). Together, these findings demonstrate that cAMP activates Epac-Rap1 and PKA signaling pathways in NRCMs.

Activation of Epac Signaling Leads to Cx43 Accumulation at Cell–Cell Contacts

Because we observed Rap1 activation in response to dbcAMP, we proceeded to investigate the involvement of Epac-Rap1 signaling in cAMP-induced Cx43 accumulation at cell–cell contacts. Like dbcAMP, 8CPT significantly enhanced the accumulation of Cx43 at the cell–cell contacts (Figure 4A and 4B). 8CPT induced Cx43 accumulation at the cell–cell contacts to a similar extent to dbcAMP and to a greater extent than 6Bnz. 6Bnz only slightly increased the number of Cx43 puncta (Figure 4B) compared with vehicle and did not further increase the accumulation of Cx43 at cell–cell contacts caused by 8CPT alone. These results indicate that Epac-mediated signaling is mainly responsible for cAMP-induced Cx43 accumulation at the cell–cell contacts.

We excluded the possibility that increased synthesis of Cx43 on cAMP stimulation resulted in the accumulation of Cx43 at the cell–cell contacts. No discernible increase was observed in the cells stimulated with vehicle, dbcAMP, 8CPT, 6Bnz, and a combination of 8CPT and 6Bnz for 12 hours (Figure 4C and 4D), suggesting that distribution or functional augmentation of GJs is essential for cAMP-induced functional GJ neoformation. In addition, phosphorylation of Cx43 was not affected by dbcAMP, 8CPT, or 6Bnz, nor a combination of 8CPT and 6Bnz (Figure 4C and 4E).

Epac Enhances AJ Formation

Several lines of evidence suggest that AJ formation organized by N-cadherin is a prerequisite for GJ assembly in cardiomyocytes when reassembling and recoupling.[26–28] We used reassembling NRCMs before drug treatment. Recently, we and others revealed that Rap1 is involved in the cell–cell contacts mediated by epithelial (E)-cadherins and vascular